J. Fluid Mech. (2002), *vol.* 472, *pp.* 333–371.
DOI: 10.1017/S0022112002002379 Printed in the United Kingdom

Polydisperse particle-driven gravity currents

By THOMAS C. HARRIS[1], ANDREW J. HOGG[2] AND HERBERT E. HUPPERT[1]

[1]Institute of Theoretical Geophysics, Department of Applied Mathematics and Theoretical Physics, University of Cambridge, Silver Street, Cambridge CB3 9EW, UK

[2]Centre for Environmental and Geophysical Flows, School of Mathematics, University of Bristol, University Walk, Bristol BS8 1TW, UK

(Received 15 August 2000 and in revised form 22 July 2002)

The intrusion of a polydisperse suspension of particles over a horizontal, rigid boundary is investigated theoretically using both an integral ('box') model and the shallow-water equations. The flow is driven by the horizontal pressure gradient associated with the density difference between the intrusion and the surrounding fluid, which is progressively diminished as suspended particles sediment from the flow to the underlying boundary. Each class of particles in a polydisperse suspension has a different settling velocity. The effects of both a discrete and continuous distribution of settling velocities on the propagation of the current are analysed and the results are compared in detail with results obtained by treating the suspension as monodisperse with an average settling velocity. For both models we demonstrate that in many regimes it is insufficient to deduce the behaviour of the suspension from this average, but rather one can characterize the flow using the variance of the settling velocity distribution as well. The shallow-water equations are studied analytically using a novel asymptotic technique, which obviates the need for numerical integration of the governing equations. For a bidisperse suspension we explicitly calculate the flow speed, runout length and the distribution of the deposit, to reveal how the flow naturally leads to a vertical and streamwise segregation of particles even from an initially well-mixed suspension. The asymptotic results are confirmed by comparison with numerical integration of the shallow-water equations and the predictions of this study are discussed in the light of recent experimental results and field observations.

1. Introduction

Particle-driven gravity currents occur when a suspension of particles intrudes into a less dense ambient fluid. In this study we consider the propagation of a relatively dense intrusion along a horizontal, rigid boundary underlying the ambient fluid. The motion is predominantly driven by the pressure gradient associated with the density difference between the suspension and the ambient, which, provided the effects of viscosity are negligible, is balanced by the inertia of the intruding fluid. Particle-driven gravity currents have received considerable attention during recent years (see the review of Huppert 1998). Studies have adopted both experimental and theoretical approaches to elucidate the physical processes which control these flows (e.g. Bonnecaze, Huppert & Lister 1993; Hallworth, Hogg & Huppert 1998). There are many examples of particle-driven flows in natural and industrial settings. These include volcanic ash flows (Sparks *et al.* 1997), turbidity currents in the ocean (Simpson 1997) and the particle-laden plumes arising from water-injection dredging (Hallworth *et al.* 1998).

Particle-driven gravity currents are dissimilar from those driven by compositional difference in fluids because the suspended particles, which contribute to the excess density, sediment to the underlying boundary as the flow evolves. Thus the density difference is progressively reduced and the flow eventually ceases, leaving a deposit of particles on the boundary. In almost all of the analytical work to date it has been assumed that the suspension of particles possess a single settling velocity. However in many situations this is a considerable simplification and in virtually all real situations there is a range of particle sizes, and hence settling velocities. For example, it has been noted that the presence of a small fraction of fine particles has a marked effect on the propagation of the particle-driven current at late stages (Harris, Hogg & Huppert 2001). Also, in many geological situations, there will be a large range of different classes of particles. For instance pyroclastic flows involve particle size ranges from tens of centimetres to microns. Similarly, turbidities comprise significant fractions of sand, silt and clay particles, the settling velocity of which differs by many orders of magnitude. Observations of long-runout turbidite deposits have indicated that a single event may lead to a segregation of grain sizes, as discussed recently by Wynn *et al.* (2002). The proximal regions comprise coarse grains in a wedge-shaped deposit which are overlain by a layer of finer particles. Conversely the distal deposits are primarily composed of the finer grained sediment.

A preliminary study of a bidisperse suspension (Dade & Huppert 1995) revealed that the effect of the smaller particles is to extend and hence thin the current more rapidly than a monodisperse suspension with the same average settling velocity. This model is only rigorously applicable, though, when the sizes of the two particle types are fairly similar. A more complete analysis, which employs the shallow-water equations, has been used to predict the deposit produced by polydisperse currents (Bonnecaze, Huppert & Lister 1996). In addition to some numerical solutions they derive a semi-analytical representation of the distribution of the deposit. This representation arises from treating the particle-laden current as monodisperse with particles of the average settling velocity. Such monodisperse flows are well-studied and Bonnecaze *et al.* (1996) fit an empirical expression for the shape of the deposit as a function of downstream distance. Since each type of particle sediments with its own settling velocity, Bonnecaze *et al.* (1996) sum appropriately weighed combinations of the distribution of the deposit to obtain an approximate expression for the overall deposit. What this theory omits is the possibility that different sedimentation rates may affect the dynamics of the current. Nevertheless comparison with numerically integrated solutions to the shallow-water equations for a range of polydisperse currents indicates that this approximation works fairly well. Part of the aim of this study is to reveal the theoretical basis for this approach and the range of its validity.

A recent set of laboratory experiments in which dilute suspensions made of two particle sizes were released into relatively shallow water has been conducted by Gladstone, Philips & Sparks (1998). They find that the presence of fine particles significantly extends the flow. Gladstone & Woods (2000) propose that a simple 'box' model, which incorporates a modified Froude number condition at the nose, provides a good model for the propagation over several multiples of the initial length of the current.

The aim of this paper is to investigate the similarities and differences that are produced when a gravity current is driven by such a polydisperse distribution of particles, rather than particles of a single size. We analyse mathematical models of the flow, using the expansion techniques developed for monodisperse flows (Harris *et al.* 2001). From the analysis, we discover that the approach of Bonnecaze *et al.*

(1996) is equivalent to the inclusion of only two terms in an appropriate Taylor series expansion. However, we also find that other statistics of the particle distribution may play an important role in characterizing the runout of some suspensions. In this paper we first present a 'box' model analysis of polydisperse gravity currents (§ 2). This extends the studies of Dade & Huppert (1995) and Gladstone & Woods (2000) and reveals when it is appropriate to model a polydisperse suspension by a monodipserse suspension with an average settling velocity. In § 3, we consider the shallow-water model of gravity current motion. This permits the resolution of the internal characteristics of the flow. By recasting the equations in terms of new independent variables and by forming Taylor series expansions for the dependent variables, we are able: to deduce how to characterize the behaviour of the current as a function of the particle distribution; to derive approximate expressions for the velocity and height profiles, which obviate the need for numerical integration of the governing equations; and to elucidate why 'box' models work so well. We confirm the asymptotic analysis by comparison with results from the numerical integration of the shallow-water equations. We find that the asymptotic results accurately reproduce the evolution of the flow until only a relatively small proportion of the initial suspended particles remains in the flow. Finally in § 4, we discuss the new results in the light of the experiments by Gladstone *et al.* (1998) and some recent field observations of Wynn *et al.* (2002). We also include an Appendix in which we develop the analysis for a continuous distribution of particle sizes.

2. Polydisperse box model

We study the gravity current formed by the intrusion of a suspension of polydisperse particles over a horizontal boundary. We assume that the suspension is sufficiently dilute for the effects of particle–particle interactions to be insignificant. A concentrated flow may behave differently. For example, Hallworth & Huppert (1998) found that particle-laden flows with initial volumetric concentrations of particles in excess of 0.15 exhibit significant differences in their dynamical behaviour from dilute flows. We assume that the particle Reynolds numbers of the suspended particles are much less than unity and hence neglect the effects of the inertia of the particles. The timescale of the response of the particle velocity to changes in the interstitial velocity field is then much shorter than the timescale on which the velocity field itself changes. We also assume that each particle is advected horizontally by the buoyancy-driven flow and sediments vertically with a constant settling velocity.

We consider a polydisperse suspension in which there are n different classes of particles. (We obtain specific results for the somewhat simpler case of a bidisperse suspension in § 2.1 and for a continuous distribution of particle sizes in Appendix A.) We denote the volume fraction and density of the ith class of particles by ϕ_i and ρ_{pi}, respectively. The reduced gravity of the suspension is therefore given by

$$g' = g \sum_{i=1}^{n} \alpha_i \phi_i, \tag{2.1}$$

where $\alpha_i \equiv (\rho_{pi} - \rho_a)/\rho_a$ is the density of the ith class of particles relative to the density of the ambient fluid. In this section in order to develop ideas and obtain simple, but powerful, analytical relationships, we adopt a 'box' model approach for modelling gravity current motion and hence propose evolution equations for integral, or horizontally averaged, properties of the current. (A shallow-water model, which

resolves the internal structure of the dynamics, is presented in § 3.) We thus consider the evolution of the length, $l(t)$, and height, $h(t)$, of the intrusion as well as the volume fraction of each class of suspended particles, $\phi_i(t)$. The equations which govern the motion are analogous to those for a monodisperse current (see Harris *et al.* 2001). On the assumption that there is no entrainment of ambient fluid into the gravity current, we may write

$$hl = A, \tag{2.2}$$

where A is the volume of the current per unit width. The speed of the front of the current is given by the Froude number condition (Benjamin 1968). In this study we assume that the dense, particle-laden fluid is intruding through a much deeper ambient fluid. Thus we may neglect the motion of the overlying ambient and the Froude number takes a constant value. Huppert & Simpson (1980) suggest that the Froude number is equal to 1.2, although the structure of the analysis which follows does not depend crucially upon this value. Hence we write

$$\frac{\mathrm{d}l}{\mathrm{d}t} = Fr(g'h)^{1/2}, \tag{2.3}$$

where Fr denotes the Froude number. Finally we specify evolution equations for the volume fractions of each class of particles. Following studies of sedimentation from turbulent suspensions (Martin & Nokes 1998) and the models of monodisperse particle-driven currents (Bonnecaze *et al.* 1993), we assume that the particles remain well-mixed throughout the depth of the current and that they settle to the underlying boundary at a known settling velocity, v_{si}, for each particulate class. In this model we neglect the re-entrainment of deposited particles into the current. (Erosive flows have been recently studied by Eames *et al.* 2001.) Hence the evolution of each volume fraction is given by

$$\frac{\mathrm{d}\phi_i}{\mathrm{d}t} = -\frac{v_{si}\phi_i}{h}. \tag{2.4}$$

To this system of equations we add the initial conditions that the current starts with vanishing initial length, and a specified volume fraction for each class of particles. Thus

$$l = 0 \quad \text{and} \quad \phi_i = \phi_i(0) \quad \text{at} \quad t = 0. \tag{2.5}$$

Note that these initial conditions, together with (2.2), causes the initial height to become infinite. However, it has been shown in previous studies (e.g. Hogg, Ungarish & Huppert 2000) that provided the final runout of these currents far exceeds the initial length, then it is an acceptable approximation to enforce $l = 0$ as an initial condition. (It is also possible to employ a non-zero initial condition for the current but the clarity of the analysis which follows is significantly reduced.)

In order to highlight the essential aspects of the analysis, we render (2.2)–(2.4) dimensionless by scaling lengths with respect to $A^{1/2}$ and times with respect to $(A^{1/2}/g_0')^{1/2}$, where g_0' is the initial volume fraction. Furthermore we introduce a scaled volume fraction given by

$$\psi_i = \frac{\alpha_i\phi_i}{\sum_{j=1}^{n}\alpha_j\phi_j(0)}. \tag{2.6}$$

Eliminating $h(t)$ from (2.2)–(2.4) and assuming $l(t)$ now denotes the dimensionless

length, we find that the governing equations are given by

$$l^{1/2}\frac{\mathrm{d}l}{\mathrm{d}t} = Fr\left(\sum_{i=1}^{n}\psi_i\right)^{1/2}, \tag{2.7}$$

$$\frac{\mathrm{d}\psi_i}{\mathrm{d}t} = -\beta_i\psi_i l, \tag{2.8}$$

where the dimensionless settling velocities are given by $\beta_i = v_{si}/[A^{1/2}g_0']^{1/2}$. These equations contain the most important feature of polydisperse flows: the current is driven by the sum of the contributions to the buoyancy force from each of the different particle types (2.7), while the volume fraction of each different particle type decays according to the individual dimensionless settling speed of that class of particles (2.8).

To analyse this system of equations, we first define an average settling velocity. The reason for introducing an average settling velocity is to investigate whether the runout of the polydisperse systems may be approximated by an 'equivalent' monodisperse current. (Such an approach has been employed by Bonnecaze *et al.* 1996.) We shall see later that the range of validity of this approximation is governed by the magnitude of the initial variance of the particle distribution. At onset, the loss of suspended sediment per unit length $\delta\psi_i$ in a dimensionless time δt is given by

$$\delta\psi_i = -\beta_i\psi_i(0)\delta t, \tag{2.9}$$

and the total loss of sediment per unit length by

$$\sum_{i=1}^{n}\delta\psi_i = -\delta t\sum_{i=1}^{n}\beta_i\psi_i(0). \tag{2.10}$$

This shows that the early behaviour of a polydisperse current will be the same as a monodisperse current with an average settling velocity $\bar{\beta}$, where $\bar{\beta}$ is defined by

$$\bar{\beta} = \sum_{i=1}^{n}\beta_i\psi_i(0). \tag{2.11}$$

Hence in dimensional terms, we define an average settling velocity, $\bar{v}_s$, which is given by

$$\bar{v}_s = \frac{\sum_{i=1}^{n} v_{si}\alpha_i\phi_i(0)}{\sum_{i=1}^{n}\alpha_i\phi_i(0)}. \tag{2.12}$$

Note that this quantity is somewhat different from the average sedimentation speed of the suspension, although the two are identical if the densities of all the classes of particulate are identical. It is nevertheless convenient to define $\bar{\beta}$ by (2.11) because the natural timescale for the evolution of the current is based upon the initial reduced gravity of the suspension.

To proceed, we rescale these polydisperse equations using the box-model scalings for a monodisperse current presented by Harris *et al.* (2001) with $\bar{\beta}$ in place of the single dimensionless settling velocity in the monodisperse study. These scalings render the runout length of the monodisperse current to be unity. In this way we are able to investigate whether polydisperse currents may be accurately represented by monodisperse currents with an appropriate average settling velocity. We re-scale the

dimensionless length and times in the evolution equations (2.7) and (2.8) by

$$l \sim \left(\frac{5Fr}{\bar{\beta}}\right)^{2/5} \quad \text{and} \quad t \sim \frac{2}{\bar{\beta}}\left(\frac{5Fr}{\bar{\beta}}\right)^{-2/5}. \tag{2.13}$$

Writing $S(t) = [l(t)]^{5/2}$, we obtain the evolution equation for the length of the current,

$$\frac{\mathrm{d}S}{\mathrm{d}t} = S^{2/5}\gamma(S), \tag{2.14}$$

where

$$\gamma(S) = \left(\sum_{i=1}^{n} \psi_i(S)\right)^{1/2}. \tag{2.15}$$

In this expression we have treated the volume fractions as functions of $S(t)$. Each of the individual volume fractions is given from (2.8) by the solution of

$$\frac{\mathrm{d}\psi_i}{\mathrm{d}S} = -2\psi_i V_i/\gamma(S), \tag{2.16}$$

where $V_i = \beta_i/\bar{\beta}$.

To obtain a first insight into how a polydisperse suspension affects the length of the current it is instructive to determine the form of $\gamma(S)$ for small values of S. We expand both $\gamma(S)$ and $\psi_i(S)$ as Taylor series in S, noting that for a monodisperse current we obtain the exact results $\psi = (1-S)^2$ and $\gamma(S) = 1 - S$. For polydisperse currents, we obtain

$$\gamma(S) = 1 - S + \sigma^2 S^2 + O(S^3), \tag{2.17}$$

where σ^2 is the initial variance of the distribution of settling velocities relative to the square of the mean settling velocity,

$$\sigma^2 = \sum_{i=1}^{n} (V_i - 1)^2 \psi_i(0). \tag{2.18}$$

The maximum length attained by the current, termed the runout length, is determined by the solution to $\gamma(S) = 0$ and below we demonstrate how this may be calculated as a function of statistics of the initial distribution of particles. From (2.17), we also note that for sufficiently small values of S, $\gamma(S) = 1 - S + O(S^2)$ and so the current behaves like a monodisperse current with an effective settling velocity $\bar{\beta}$. Thus, during the early phases of the flow it is adequate to approximate the polydisperse current by a monodisperse current with the average settling velocity of the particles. However as the length of the current increases, this approximation becomes invalid. The effects of a distribution of particle sizes will be first observed when $\sigma^2 S^2 = O(1)$. Since we have rescaled the length of the current so that runout is such that $S = O(1)$, we may conclude that a polydisperse current behaves like a monodisperse current of average settling velocity when

$$\sigma^2 \ll 1. \tag{2.19}$$

This is an important result for discriminating between different flows. Currents created in the laboratory will always contain particles of different settling velocities due to slight differences in shape and size. By calculating the variance of the distribution of settling velocities we can check whether the current may be effectively modelled as monodisperse. For polydisperse suspensions with a much larger variance, we are

interested in what effects are produced by other statistics of the particle distribution as explained below.

To commence, we note that the unknown function $\gamma(S)$ may be eliminated from (2.16) by dividing the equation for one volume fraction by another. Thus each of the individual volume fractions may be expressed in terms of just one new unknown function. The result, which can be verified by direct substitution, is

$$\psi_i(S) = \psi_i(0)a(S)^{V_i}, \tag{2.20}$$

where the unknown function $a(S)$ satisfies the same equation as derived for the monodisperse box model,

$$\frac{\mathrm{d}a}{\mathrm{d}S} = -2a(S)/\gamma(S), \tag{2.21}$$

with

$$\gamma(S) = \left(\sum_{i=1}^{n} \psi(0)a(S)^{V_i}\right)^{1/2}. \tag{2.22}$$

Thus for a bidisperse suspension, if the ratio of the settling velocities is R, then the volume fraction of the heavier particles decays R times faster than that of the lighter particles. This result was noted by Dade & Huppert (1995), although their subsequent analysis is somewhat different. In § 3, we shall see that a similar and more powerful result also holds true for the shallow-water equations.

We note that the maximum extent of the current, $S_m^{2/5}$, is given when $a = 0$. Hence

$$S_m = \frac{1}{2}\int_0^1 \frac{\left(\sum_{i=1}^{n} \psi_i(0)a^{V_i}\right)^{1/2}}{a}\,\mathrm{d}a. \tag{2.23}$$

By substituting $a = \exp(-2y)$, this may be written

$$S_m = \int_0^\infty \left(\sum_{i=1}^{n} \psi_i(0)\exp\left(-2V_i y\right)\right)^{1/2}\mathrm{d}y. \tag{2.24}$$

Recall that $\sum_{i=1}^{n} \psi_i(0) = 1$ and $\sum_{i=1}^{n} \psi_i(0)V_i = 1$, so that the integral may be expanded in terms of moments of the initial distribution of particles. We find that

$$S_m = 1 + 2M_2 - 4M_3 + 4(2M_4 - 3M_2^2) + \cdots, \tag{2.25}$$

where $M_n = \sum_{i=1}^{n} \psi_i(0)(V_i - 1)^n$.

It is also a straightforward task to integrate (2.21) numerically for any given initial distribution of particles to determine the function $a(S)$ and thereby all the volume fractions as functions of the distance propagated. A further numerical integration of (2.14) can then be performed if the evolution of the current length as a function of time is required.

Alternatively, we may use an iterative scheme, as described in Harris *et al.* (2001), to generate approximations for the length and volume fractions as functions of time. As we do not have analytic expressions for the volume fractions, for each iterate we have to solve (2.16) first and then use this approximation in (2.15). The method for deriving the results is identical to the monodisperse box model (Harris *et al.* 2001).

Writing $\tau = (3t/5)^{5/3}$ and denoting the iterates for S and ψ_i by S_n and ψ_{in}, we find

$$\frac{\mathrm{d}}{\mathrm{d}\tau}\left(\tfrac{5}{3}S_n^{3/5}\right) = \tau^{-2/5}\gamma(S_{n-1}, \psi_{n-1}), \tag{2.26}$$

$$\frac{\mathrm{d}}{\mathrm{d}\tau}(\log\,\psi_{in}) = -2V_i S_{n-1}^{2/5}. \tag{2.27}$$

Starting from $S_0 = 0$ and $\psi_0 = 1$, we obtain the first iterates

$$S_1(t) = \tau \quad \text{and} \quad \psi_{i1}(t) = \psi_i(0)\exp(-2V_i\tau). \tag{2.28}$$

The result for ψ_{i1} expresses the fact that for small times each different particle type sediments independently, as if it were from a homogeneous current. This follows because at early times the decrease in the driving buoyancy force caused by sedimentation has not yet influenced the development of the current. Calculating the second iterate, we obtain

$$S_2(t) = \left[\frac{3}{5}\int_0^\tau \tau'^{-2/5}\left(\sum_{i=1}^n \psi_i(0)\exp(-2V_i\tau')\right)^{1/2}\mathrm{d}\tau'\right]^{5/3}. \tag{2.29}$$

Since each settling velocity produces a different rate of exponential decay, it is not possible to represent this approximation in terms of gamma functions, as was possible for the monodisperse currents (cf. Harris *et al.* 2001). We may obtain a good approximation to the third iterate by making a Taylor series expansion of the decaying exponential term as employed in Harris *et al.* (2001). This enables us to write down the following approximation of the current length $\tilde{l}(t)$:

$$\tilde{l}(t) = \left[\frac{3}{5}\int_0^\tau \tau'^{-2/5}\left(\sum_{i=1}^n \psi_i(0)(1 + V_i\tau'^2/4)\,\exp(-2V_i\tau')\right)^{1/2}\mathrm{d}\tau'\right]^{2/3}. \tag{2.30}$$

This expression is more complicated than the simple expressions derived in terms of gamma functions for monodisperse currents. However, it can be integrated numerically for any initial distribution of particles.

The deposit arising from the passage of these particle-driven flows may be simply calculated as follows. In terms of dimensional variables, the distribution of the mass per unit area is given

$$\eta(x) = \int_{t_*}^\infty \sum_{i=1}^n \rho_{pi} v_{si}\phi_i(t)\,\mathrm{d}t, \tag{2.31}$$

where t_* is defined by $l(t_*) = x$ and corresponds to the time at which the current first reaches a downstream location x. In the expression above, observe that the deposit depends on the sum of the deposition from each of the classes of particles. On the assumption that the densities of each class of particles are identical, we render the deposit, η, dimensionless with respect to $\rho_p A^{1/2}$ and further re-scale by a factor $(2/\bar{\beta})(5Fr/\bar{\beta})^{-2/5}$ (cf. (2.13)). Next we change the variable of integration to S and denote the re-scaled dimensionless distance and deposit by X and Y, respectively to

obtain the distribution of the deposit,

$$\Upsilon(X) = \int_{S_*}^{S_m} \frac{\sum_{i=1}^{n} V_i \psi_i}{S^{2/5} \left[\sum_{i=1}^{n} \psi_i\right]^{1/2}} \, \mathrm{d}S, \tag{2.32}$$

where $S_* = X^{5/2}$ and S_m corresponds to the runout length of the gravity current, given by $\gamma(S_m) = 0$. Note that the assumption of identical particle densities serves only to simplify the analysis and need not be invoked.

2.1. *Bidisperse currents*

So far the analysis has been for a general polydisperse gravity current in which there are n different class of particles. We now examine the box-model solutions when there are just two classes of particles with different settling velocities. We have already noted that the crucial difference between poly- and monodisperse currents is that the rate of sedimentation is different for each of the classes of particles. The more slowly sedimenting particles mean that the excess density of the current is maintained over a longer distance and hence the current propagates further than predicted if it had been treated as monodisperse with the average settling velocity of suspension. We have also noted that this effect is more pronounced if the variance of the initial distribution of settling velocities is large compared to the square of the mean settling velocity. For bidisperse currents it is possible to make further analytical progress, which we pursue in this section. (We compare some of the deductions from this analysis with some of the deductions arising from the experimental study of Gladstone *et al.* 1998 in § 4.)

We assume that the re-scaled volume fractions of particles are given by

$$\psi_1 = f \quad \text{and} \quad \psi_2 = 1 - f, \tag{2.33}$$

where $0 \leqslant f \leqslant 1$. Furthermore the ratio of the dimensionless settling velocities is given by $\beta_2/\beta_1 = \lambda$, and $\lambda < 1$ on the assumption that the first class of particles has a greater settling velocity than the second. (Assuming the particles are of the same density, we shall refer to the first class as the *coarse* particles and the second as the *fine* particles.) The variance of the settling velocities in the suspension is initially given by

$$\sigma^2 = \frac{f(1-f)(1-\lambda)^2}{[f + \lambda(1-f)]^2}. \tag{2.34}$$

We note that the variance vanishes, as it must, if the particles have identical settling velocities $\lambda = 1$, of if we have entirely one class or other ($f = 0$ or $f = 1$). Furthermore the variance is maximized when $f = \lambda/(1+\lambda)$.

The runout length of the gravity current, $S_m^{2/5}$, is given by the solution to $\gamma(S_m) = 0$. Hence from (2.21) we obtain

$$S_m = \frac{1}{2} \int_0^1 \left(f a^{V_1} + (1-f) a^{V_2}\right)^{1/2} a^{-1} \, \mathrm{d}a. \tag{2.35}$$

This integral may be re-written as

$$S_m = \frac{f + (1-f)\lambda}{\lambda} \, {}_2F_1\left(-\tfrac{1}{2}, 1; 1 + \frac{\lambda}{2(1-\lambda)}; f\right), \tag{2.36}$$

where ${}_2F_1$ denotes a hypergeometric function (Abramowitz & Stegun 1964).

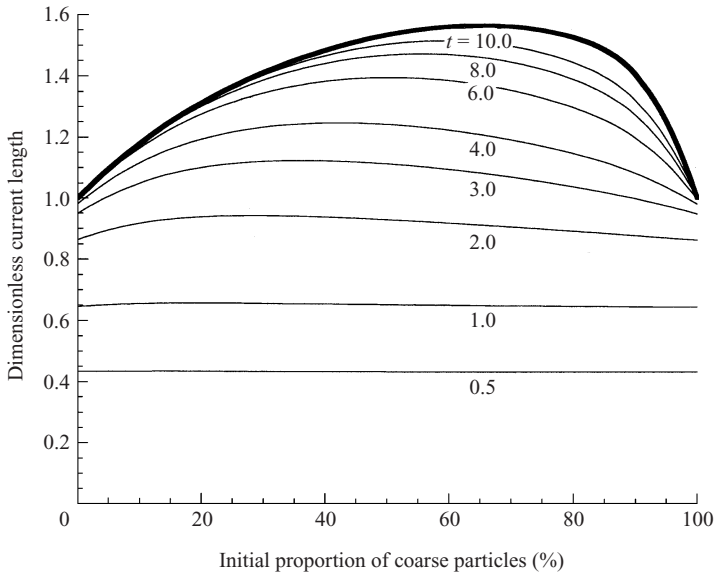

FIGURE 1. The dimensionless, rescaled length $l/[5FrA(g_0'A)^{1/2}/\bar{\beta}]^{2/5}$ of a particle-driven gravity current containing a bidisperse distribution of particles with a $7:1$ ratio of settling velocities as a function of the proportion of coarse particles (f). The thick line shows the final runout length attained by the current. The thin lines show the length at dimensionless times $t = 0.5, 1, 2, 3, 4, 6, 8, 10$. Note that if plotted in terms of dimensional variables then the maximal length of the current would decrease monotonically with increasing initial coarse fraction.

We illustrate these results by considering a bidisperse suspension in which the settling velocities have a $7:1$ ratio. We plot in figure 1 the runout length $l_m \equiv [S_m]^{2/5}$ as a function of the proportion of coarse particles. It is important to recall that this runout length has been non-dimensionalized with respect to that which is predicted using the average settling velocity. Hence when there is solely coarse, or fine, particles ($f = 0$, or $f = 1$), we find that $l_m = 1$. Whenever there is a mixture of particles $l_m > 1$. This reflects our earlier conclusion that any degree of polydispersion increases the runout of the gravity currents.

Figure 1 also shows how these currents evolve towards the final runout distance as we plot the length at a few given times as a function of the proportion of coarse particles. Note that at early times there is no difference in the distance propagated by the bidisperse gravity currents with any proportion of coarse particles. This reflects the observation that the early behaviour of the current is well-represented by a monodisperse current with the average settling velocity. However as time progresses we begin to notice differences. For this case ($\lambda = 1/7$), the greatest propagation occurs when $f = 0.65$

In figure 2 we plot the length of the current as a function of time for a few chosen values of the proportion of coarse particles. Once again we observe how the early time behaviour is independent of the precise proportion of fine particles, but as time progresses the curves begin diverge. We also plot the approximate solution (2.30) for the evolution of the current length and note that the approximate solution works reasonably well.

For bidisperse gravity currents the dimensionless distribution (2.32) of the deposit is given by

$$\Upsilon(X) = \int_{S_*}^{S_m} \frac{\left[V_1 f a^{V_1} + V_2(1-f)a^{V_2}\right]}{S^{2/5}\left[f a^{V_1} + (1-f)a^{V_2}\right]^{1/2}}\,\mathrm{d}S, \tag{2.37}$$

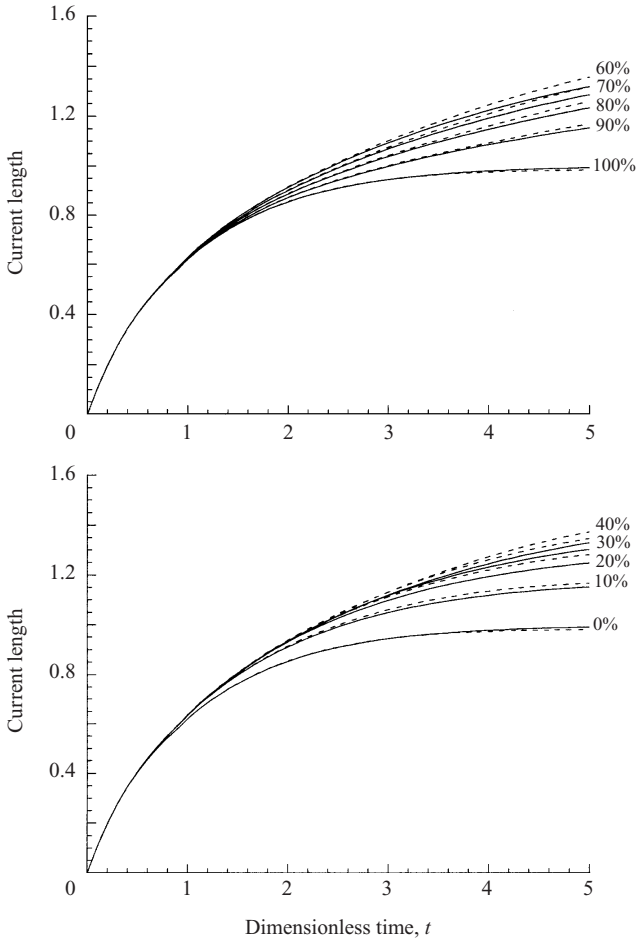

FIGURE 2. The non-dimensional length of particle-driven gravity current (l) containing a bidisperse distribution of particles with a 7 : 1 ratio of settling velocities as a function of dimensionless time t. Curves are shown for a range of initial proportions of coarse particles. Also plotted are the approximate solutions derived from (2.30) for the length as a function of time $\tilde{l}(t)$ (- - - -).

where $a(S)$ satisfies (2.21). We integrate this expression for $\lambda \equiv V_2/V_1 = 1/7$ and a range of values of f and present the results in figure 3. In these plots we show the contributions to the depth of deposit from both the fine and coarse particles. Note that both contributions thin with distance from the point of release, with the deposit near the source being relatively rich in the coarse particles compared to that in the distal regions. It is noteworthy, though, that the spatial scale is different for each of these flows because distances are scaled by $\bar{\beta}^{-2/5}$. To enable comparison between the cases we scale the dimensionless distance l with respect to $(5Fr/\beta_1)^{2/5}$, rather than $(5Fr/\bar{\beta})^{2/5}$. With this scaling the spatial scale remains invariant for each of the calculations of the depth of the deposit (figure 4). Thus we note that increasing the proportion of fine particles leads to the coarse particles being deposited over a greater downstream distance.

Finally we calculate the proportion of coarse sediment within the deposit. This provides an indication of the lateral segregation of different sediment types within the deposit from an initially well-mixed suspension. The dimensionless flux of coarse

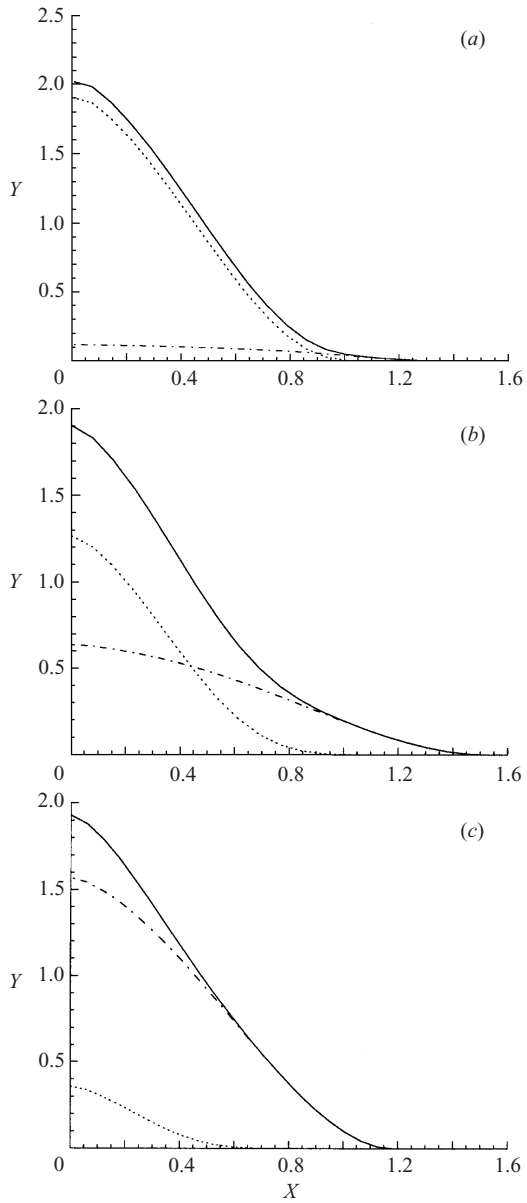

FIGURE 3. The distribution of the deposit arising from sedimentation from a bidisperse particle-driven gravity current. The total depth of the deposit is plotted (———), which comprises contributions from both the fine (— · — ·) and coarse fractions (- - - -) of particles. The deposit is shown for initial coarse fractions of (*a*) 90%, (*b*) 50%, (*c*) 10%.

sediment to the underlying deposit is given by $V_1\psi_1$ and hence the proportion of coarse sediment is given by

$$\mathscr{P}(t) = \frac{V_1\psi_1}{V_1\psi_1 + V_2\psi_2}. \tag{2.38}$$

Thus $\mathscr{P}$ is a decreasing function of time, with initial value

$$\mathscr{P}(0) = \frac{f}{f + (1-f)\lambda}. \tag{2.39}$$

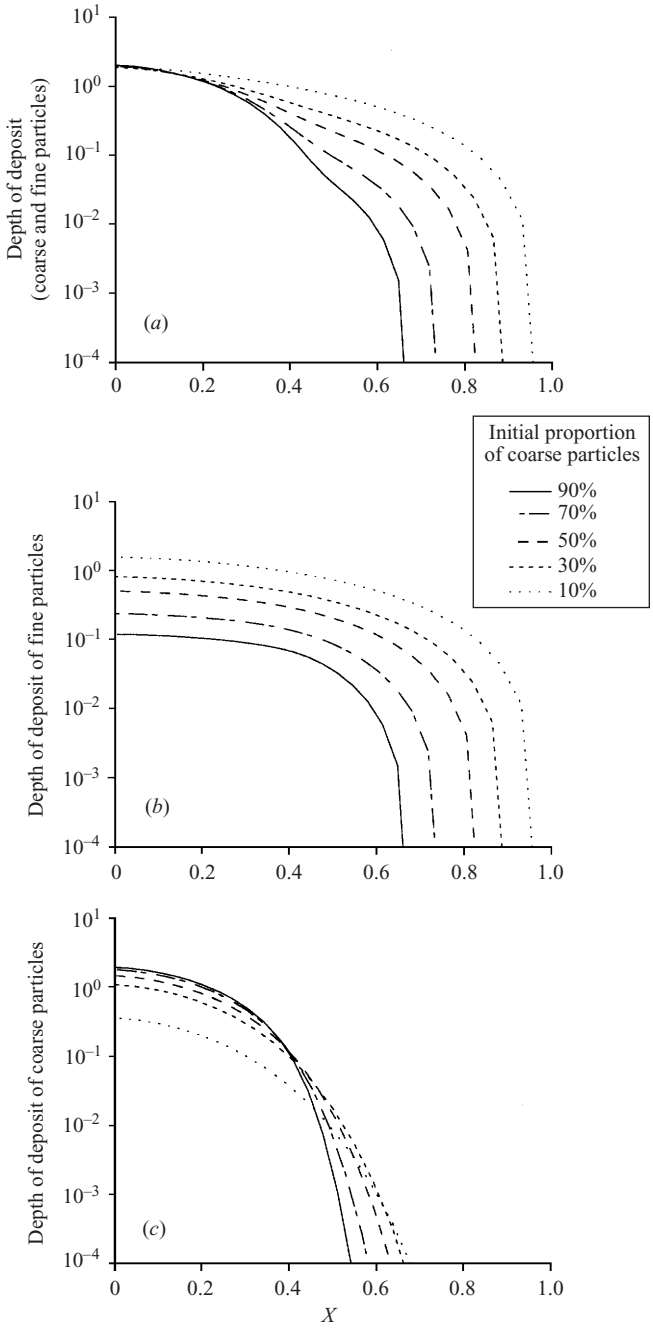

FIGURE 4. The distribution of the deposit arising from sedimentation from a bidisperse particle-driven gravity current. The figures show (*a*) total depth of the deposit; (*b*) the depth of fine particles; and (*c*) the depth of coarse particles. The dimensionless distance has been rescaled so that it is identical for each of the initial proportions of coarse particles.

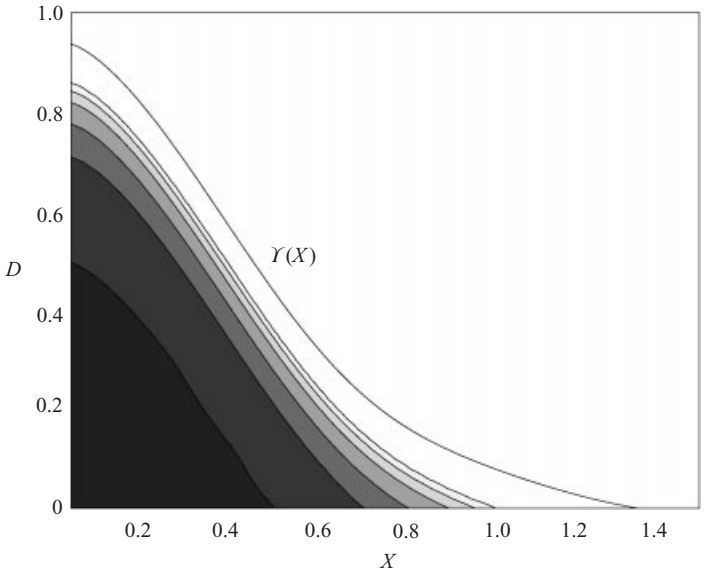

FIGURE 5. The distribution of the deposit and the proportions of coarse and fine particles within it arising from sedimentation from a bidisperse particle-driven gravity current. In this calculation, $V_2/V_1 = 1/7$ and the suspension initially contains equal proportions of fine and coarse particles ($f = 0.5$). The contours are shown for 80%, 60%, 40%, 20%, 10% and 5% of coarse particles within the deposited material. Also shown is the total depth of the deposit, $\Upsilon(X)$, as a function of downstream distance (———).

We may also formulate an expression for the way in which the deposit grows in time. Denoting the dimensionless depth of deposit at a downstream distance X and at time t, by $D(X,t)$, we find that

$$D(X,t) = \int_{S_*}^{S(t)} \frac{\left[V_1 f a^{V_1} + V_2(1-f)a^{V_2}\right]}{S^{2/5}\left[f a^{V_1} + (1-f)a^{V_2}\right]^{1/2}}\,\mathrm{d}S \quad \text{for} \quad S(t) \geqslant S_*, \tag{2.40}$$

where $S_* = X^{5/2}$. Since we now have the depth of the deposit as a function of time and the proportion of coarse particles in the depositing flux of sediment, we may track how the proportion of coarse particles evolves with time and distance within the flow. In figure 5 we illustrate the results for a current with equal initial fractions of coarse and fine particles ($f = 0.5$), but with $\lambda = 1/7$. We note how the coarse particles preferentially settle out close to the start of the current, whereas the fine particles are advected further downstream. The nature of the deposit therefore changes in both the streamwise direction and in the vertical. The coarse particles tend to settle out first and so are overlain by a deposit which becomes progressively finer. However the deposit also fines downstream since the coarse particles predominantly sediment within a region close to the source. We may calculate the composition of the deposit as a function of the relative depth within the deposit at locations downstream of the source. For example, we plot the composition at four downstream distances ($X = 0.1, 0.4, 0.7$ and 1.0) in figure 6 and note how the profiles evolve from a banded deposit with a layer of predominantly coarse particles overlain by a layer of fine particles close to the source ($X = 0.1$), to a deposit which is almost entirely composed of fine particles at large distances from the source ($X = 1.0$). We note that at present profiles such as these are not measured in laboratory experiments, though this would be an interesting investigation.

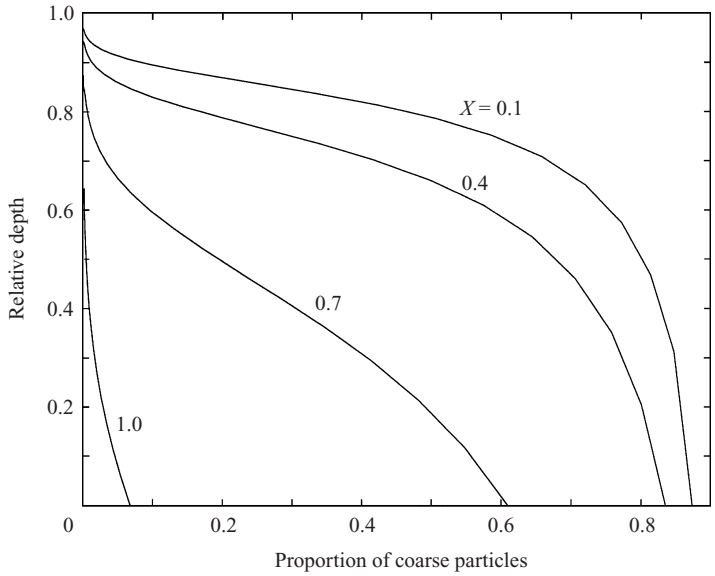

FIGURE 6. The composition of the deposit as a function of relative depth within the deposit at $X = 0.1, 0.4, 0.7$ and 1.0.

3. Polydisperse shallow-water model

While box models provide the evolution of bulk characteristics of gravity current motion, they do not resolve the internal structure of the flows. To do this we employ a system of shallow-water equations in which the dependent variables, the horizontal velocity, height of the current and volume fraction of particles, are functions of the horizontal spatial coordinate and time. This model does not resolve the vertical distribution of the velocity field and volume fraction of particles, but for monodisperse currents such a class of models has been used to accurately model the evolution of the flow. We demonstrate that many of the simple results obtained for this more complete model are similar to those obtained for the box model. The formulation of the shallow-water model is the same as that employed by, for example, Bonnecaze *et al.* (1993) and Harris *et al.* (2001). The length of the flow is assumed to be much greater than the depth so that vertical accelerations are negligible and the pressure adopts a hydrostatic distribution in the vertical. Then depth-averaged equations are formulated for the horizontal velocity field and the height of the current. In addition, the volume fraction of each class of particles is modelled on the assumptions that within the current it is vertically uniform, that the particles settle to the underlying horizontal boundary with a constant settling velocity, which is different for each particulate class and that no particles are re-entrained having been deposited on the underlying boundary. Thus the turbulence within the flow is sufficient to mix the relatively heavy particles vertically, but insufficient to erode those already deposited. This regime may be specified as follows for particles with settling velocity v_s and diameter d, moving through fluid of kinematic viscosity ν in which the magnitude of the turbulent velocities is u_*. For the particles to be vertically well-mixed, $v_s/u_* \ll 1$ and for there to be no re-entrainment of deposited particles, $v_s/u_* > (u_* d/\nu)^2$. The latter condition arises from formulating the critical Shields parameter for the threshold of motion (Fredsoe & Deigaard 1992) and by using the Stokes settling velocity for the particle. In the laboratory experiments described

below (§4), particles of size 10^{-5} m were suspended in water and their settling velocity was of order $10^{-3}\,\mathrm{m\,s^{-1}}$. We estimate the turbulent velocity fluctuations to be of order $10^{-2}\,\mathrm{m\,s^{-1}}$ and thus $v_s/u_* = 0.1$, while $(u_* d/\nu)^2 = 10^{-2}$. Hence the regime of a vertically uniform concentration field, together with no re-entrained particles, is adequately realized in laboratory experiments.

A thorough discussion of the validity of the assumptions underlying this model is given by Harris *et al.* (2001). They identify the timescales over which viscous forces begin to influence the flow and the timescales over which significant horizontal shear develops in the velocity field.

As in §2, we non-dimensionalize lengths with respect to $A^{1/2}$ and times with respect to $(A^{1/2}/g_0')^{1/2}$, where g_0' is the initial reduced gravity of the suspension. We also scale the volume fractions according to (2.6). We henceforth denote the dimensionless velocity, height and volume fraction fields by $u(x,t)$, $h(x,t)$ and $\psi_i(x,t)$, respectively. Furthermore the dimensionless length of the current is denoted $x_N(t)$ and the dimensionless settling velocities by β_i. Thus the equations for conservation of mass and momentum are

$$\frac{\partial h}{\partial t} + \frac{\partial}{\partial x}(uh) = 0, \tag{3.1}$$

$$\frac{\partial}{\partial t}(uh) + \frac{\partial}{\partial x}(u^2 h + \tfrac{1}{2}\Psi h^2) = 0, \tag{3.2}$$

where $\Psi(x,t)$ is defined as the sum of all the separate components of the volume fraction,

$$\Psi(x,t) = \sum_{i=1}^{n} \psi_i(x,t). \tag{3.3}$$

There is a separate equation describing the evolution of each of the $\psi_i(x,t)$ representing the conservation of particles of type i. In dimensionless form, these are

$$\frac{\partial \psi_i}{\partial t} + u\frac{\partial \psi_i}{\partial x} = -\frac{\beta_i \psi_i}{h}. \tag{3.4}$$

The boundary conditions for this flow are similar to those employed by Bonnecaze *et al.* (1996): no velocity at the origin, $u(0,t) = 0$; and the Froude number condition for the speed at the nose of the current, which is modified to include the effect of all the particles,

$$u(x_N,t) = Fr[h(x_N,t)\Psi(x_N,t)]^{1/2}. \tag{3.5}$$

In addition there is an expression for global conservation of volume,

$$\int_0^{x_N(t)} h\,\mathrm{d}x = 1, \tag{3.6}$$

and a condition for kinematic consistency at the front of the flow, given by

$$\frac{\mathrm{d}x_N}{\mathrm{d}t} = u(x_N(t),t). \tag{3.7}$$

To those equations and boundary conditions, we must add initial conditions for the profile and velocity of the current, but provided the runout distance of the flow far exceeds its initial length, these do not significantly influence the following results after an initial (short) adjustment time (see Hogg *et al.* 2000).

To analyse this system of equations and boundary conditions, we first rescale

length- and timescales by

$$l \sim \left(\frac{5Fr}{\bar{\beta}}\right)^{2/5} \frac{1}{b^{1/5}} \quad \text{and} \quad t \sim \frac{2}{\bar{\beta}} \left(\frac{5Fr}{\bar{\beta}}\right)^{-2/5} b^{1/5}, \tag{3.8}$$

where $\bar{\beta}$ is the average settling velocity given by (2.11) and $b = 1 - Fr^2/6$. Note that except for the factor b, these scalings are identical to those of the box model (2.13). We now introduce different independent variables, to replace x and t. These are given by

$$\xi = x/x_N(t) \quad \text{and} \quad s = [x_N(t)]^{5/2}. \tag{3.9}$$

The dependent variables are now treated as functions of ξ and s and written as

$$h(x,t) = H(\xi,s)/x_N(t), \quad u(x,t) = \frac{\mathrm{d}x_N(t)}{\mathrm{d}t} U(\xi,s) \quad \text{and} \quad \psi_i(x,t) = \varphi_i(\xi,s). \tag{3.10}$$

The resulting equations and boundary conditions are then rewritten in terms of these new variables. Importantly we obtain the following evolution equation for $s(t)$:

$$\frac{\mathrm{d}s}{\mathrm{d}t} = s^{2/5} F(s), \tag{3.11}$$

where the new function $F(s)$ is defined by the boundary condition applied at $\xi = 1$,

$$F(s) = [bH(1,s)\,\Psi(1,s)]^{1/2}. \tag{3.12}$$

Note that $F(0)$ is non-vanishing and it may be expanded as a Taylor series (see § 3.1). One of our aims is to investigate how $F(s)$ differs from that derived for a monodisperse suspension Harris *et al.* (2001). We observe that the function $F(s)$ within the shallow-water framework is analogous to the function $\gamma(S)$ within the box-model analysis. Comparison between these functions will permit an evaluation of the differences between the two models. Also, on the basis of what we have found using the box model, we expect the dynamics of polydisperse currents to be similar at first to those of a particle-laden current with the average settling velocity, $\bar{\beta}$, but at later times we must account for higher moments in the distribution of the settling velocities. Indeed it was found that the variance of the distribution came into $\gamma(S)$ at $O(S^2)$.

In terms of the new variables, the governing equations for conservation of mass and momentum are given by

$$2\frac{\partial}{\partial \xi}[(U-\xi)\,H] + 5s\frac{\partial H}{\partial s} = 0, \tag{3.13}$$

$$F^2\left[2(U-\xi)\,\frac{\partial U}{\partial \xi} + 5s\,\frac{\partial U}{\partial s}\right] - \left(F^2 - 5s\frac{\mathrm{d}F}{\mathrm{d}s}\right) U + \frac{a}{H}\,\frac{\partial}{\partial \xi}\left(\Psi H^2\right) = 0, \tag{3.14}$$

where $a = b/Fr^2$. Particle conservation is now expressed by

$$2(U-\xi)\,\frac{\partial \varphi_i}{\partial \xi} + 5s\,\frac{\partial \varphi_i}{\partial s} + \frac{10 V_i\,\varphi_i\,s}{HF} = 0, \tag{3.15}$$

where V_i is, as before, the ratio of β_i to $\bar{\beta}$. On the assumption that each class of particles has an identical initial distribution, this set of equations again admits solutions for the volume fractions as powers of a new function $\Omega(\xi,s)$. If the suspension is initially well-mixed, so that it is spatially homogeneous, each of the volume fractions can be written as

$$\varphi_i(\xi,s) = \varphi_i(0)\,\Omega(\xi,s)^{V_i}, \tag{3.16}$$

where $\varphi_i(0)$ denotes the initial uniform volume fraction of the ith class of particles and $\Omega(\xi, s)$ satisfies

$$2(U-\xi)\frac{\partial \Omega}{\partial \xi} + 5s\frac{\partial \Omega}{\partial s} + \frac{10\,\Omega s}{HF} = 0. \tag{3.17}$$

Note that this evolution equation is identical to the equation for volume fraction derived for monodisperse currents (Harris *et al.* 2001).

3.1. *Power series analysis*

Following the approach of Harris *et al.* (2001), we investigate this new system of governing equations by expanding all of the variables as power series in s. Note that the structure of the governing equations (3.13), (3.14) and (3.17) is such that these power series may only proceed in integer powers of s. Thus we write

$$H(\xi, s) = H_0(\xi) + sH_1(\xi) + s^2H_2(\xi) + \cdots, \tag{3.18}$$

$$U(\xi, s) = U_0(\xi) + sU_1(\xi) + s^2U_2(\xi) + \cdots, \tag{3.19}$$

$$\Omega(\xi, s) = 1 + s\Omega_1(\xi) + s^2\Omega_2(\xi) + \cdots, \tag{3.20}$$

$$F(s) = F_0 + sF_1 + s^2F_2 + \cdots. \tag{3.21}$$

The series expansions are then substituted into the governing equations and terms are equated in orders of s (Harris *et al.* 2001).

At $O(1)$, we recover the similarity solutions for a current of constant density propagating through a less dense ambient (see Hoult 1972; Bonnecaze *et al.* 1993; Hogg *et al.* 2000). At this order we neglect particle sedimentation ($\Omega_0 = 1$) and the velocity and height fields are given by

$$U_0(\xi) = \xi, \tag{3.22}$$

$$H_0(\xi) = (\xi^2 - 1)/4a + 1/b, \tag{3.23}$$

while from the series expansion of the evolution equation (3.12), we deduce $F_0 = 1$.

At $O(s)$, we begin to observe the effects of sedimentation in the solutions for the volume fraction, velocity and height of the current. First we find that

$$\Omega_1 = -2/H_0. \tag{3.24}$$

Hence from (3.16), by forming an expansion for φ_i, we find that

$$\varphi_{i1} = -2V_i\varphi_{i0}(0)/H_0. \tag{3.25}$$

Thus the volume fraction of each class of particles is reduced by an amount proportional to the settling velocity, relative to the average settling velocity, and to its initial value, and inversely proportional to the leading-order height of the current. This implies that the first-order correction to the total volume fraction is given by

$$\Psi_1 = \sum_{i=1}^{n} \varphi_{i1} = -2/H_0. \tag{3.26}$$

This result means that the first-order corrections to the height and velocity fields have exactly the same form as for a monodisperse current (Harris *et al.* 2001). Truncating the series at this order has reproduced mathematically the semi-analytical model of Bonnecaze *et al.* (1996). The evolution of the current is exactly the same as a monodisperse current with an appropriate average settling velocity, $\bar{\beta}$, whilst the

individual components of the volume fraction decay with their own settling velocities. The first-order velocity field satisfies

$$(4aH_0U_1)'' - 30U_1 = 15F_1\xi - \frac{10aH_0'}{H_0}, \tag{3.27}$$

subject to $U_1(0) = U_1(1) = 0$, where a prime denotes differentiation with respect to ξ. Thus the solution is given by

$$U_1(\xi) = a_2 \mathrm{i} Q_5'(\zeta) + \frac{aH_0'}{3H_0} - \tfrac{5}{8}F_1\xi, \tag{3.28}$$

where $\zeta = \mathrm{i}\xi(4a - 1/3)^{-1/2}$, Q_5 is the fifth-order Legendre function of the second kind, and a_2 and F_1 are constants which are determined by the boundary conditions and depend upon the magnitude of the Froude number, Fr. (For $Fr = 1.19$, $a_2 = -0.011$ and $F_1 = -0.578$.) The first-order height field is related to this velocity field by

$$H_1 = -2\,(U_1H_0)'/5. \tag{3.29}$$

These functions are plotted in figure 7 along with the $O(1)$ similarity solutions.

Harris *et al.* (2001) find that truncating at first order only produces good results for relatively small values of s. Fortunately we are in a position to calculate the $O(s^2)$ terms to improve upon this and to identify the effects of polydispersion. The second-order correction to the volume fraction is given by

$$\Omega_2 = (10 + 5F_1H_0 + 5H_1 - 2U_1H_0')/5H_0^2. \tag{3.30}$$

As observed above, the evolution equation for Ω is identical to that for the volume fraction in a monodisperse gravity current. Hence this second-order correction is also identical to that for a monodisperse current (see Harris *et al.* 2001). Substitution of (3.30) into (3.16) yields

$$\varphi_{i2} = V_i\varphi_i(0)(10V_i + 5F_1H_0 + 5H_1 - 2U_1H_0')/5H_0^2. \tag{3.31}$$

The only changes in this expression from (3.30) are the pre-multiplicative factor and the inclusion of an extra factor V_i inside the brackets. This means that the volume fractions of particles with a settling velocity less than the average will decay more quickly than before, whilst the converse is true for particles with settling speeds greater than the average. The second-order correction to the total volume fraction now depends upon the variance of the particle distribution,

$$\Psi_2 = \sum_{i=1}^{n} \varphi_{i2} = (10 + 10\sigma^2 + 5f_1H_0 + 5H_1 - 2U_1H_0')/5H_0^2. \tag{3.32}$$

(We note that $\sigma^2 = 0$ recovers the monodisperse result.) This extra term is always positive and hence the rate at which the total volume fraction of suspended particles declines is reduced. Hence the current always propagates further, independent of the precise details of the particle distribution. This result is entirely analogous to that obtained from the box model.

Since the modification to Ψ_2 due to polydispersion is proportional to σ^2, we deduce that the modifications to all the other second-order quantities due to polydispersion can be written as multiples of σ^2. Hence we may partition the second-order functions into parts associated with an equivalent monodisperse current ($\sigma^2 = 0$) and parts which arise when the variance is non-zero ($\sigma^2 > 0$). The monodisperse functions, denoted by $H_2|_{\sigma=0}$ and $U_2|_{\sigma=0}$, were calculated by Harris *et al.* (2001) and are plotted

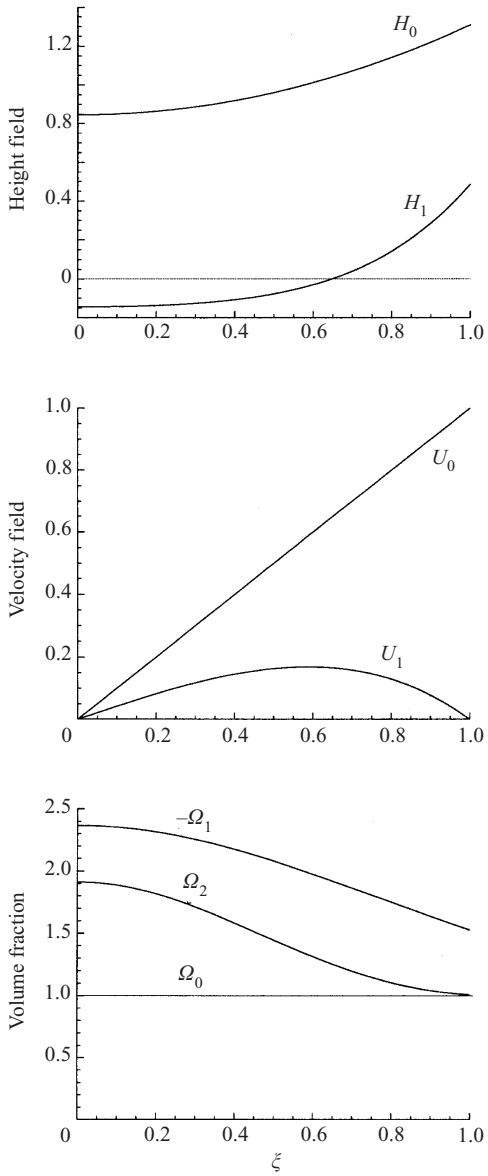

FIGURE 7. The similarity solutions $H_0(\xi)$, $U_0(\xi)$ and Ω_0, together with the first-order perturbation functions, $H_1(\xi)$, $U_1(\xi)$ and $\Omega_1(\xi)$. Also plotted is the second-order function $\Omega_2(\xi)$.

in figure 8. Furthermore $F_2|_{\sigma=0} = 0.114$ for $Fr = 1.19$. In order to analyse the contributions associated solely with polydispersivity parts, we define the parameter

$$\mathscr{F} = (F_2 - F_2|_{\sigma=0})/\sigma^2, \tag{3.33}$$

and the functions

$$\mathscr{U} = (U_2|_{\sigma\neq0} - U_2|_{\sigma=0})/\sigma^2, \tag{3.34}$$

$$\mathscr{H} = (H_2|_{\sigma\neq0} - H_2|_{\sigma=0})/\sigma^2. \tag{3.35}$$

On substitution of these functions into the governing equations, we obtain the fol-

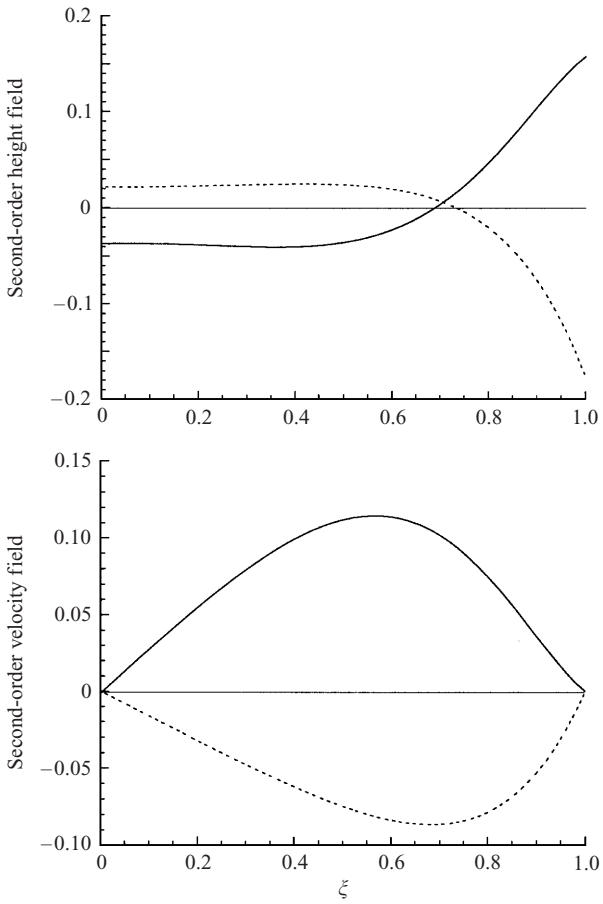

FIGURE 8. The second-order perturbation functions, $H_2(\xi)$ and $U_2(\xi)$, decomposed into contributions $H_2(\xi)|_{\sigma=0}$ (———) and $\mathscr{H}(\xi)$ (- - - -), and $U_2(\xi)|_{\sigma=0}$ (———) and $\mathscr{U}(\xi)$ (- - - -).

lowing differential equations for $\mathscr{U}$ and $\mathscr{H}$:

$$(\mathscr{U}H_0)' + 5\mathscr{H} = 0, \tag{3.36}$$

$$11\mathscr{U} + 8\mathscr{F}\xi + 2a\mathscr{H}' = 0. \tag{3.37}$$

Hence these may be combined to yield a single, second-order differential equation for $\mathscr{U}$, given by

$$(4aH_0\mathscr{U})'' - 110\mathscr{U} = 80\mathscr{F}\xi. \tag{3.38}$$

The boundary conditions on $\mathscr{U}$ are no flow at the origin, the global conservation of fluid volume, and the evolution condition at the front of the current. These may be expressed, respectively, as

$$\mathscr{U}(0) = \mathscr{U}(1) = 0 \quad \text{and} \quad \mathscr{U}'(1) = -10\mathscr{F} + 5b^2. \tag{3.39}$$

The solution may be written in terms of Legendre functions as

$$\mathscr{U}(\xi) = \mathscr{A}P'_{10}(\zeta) + \mathscr{B}Q'_{10}(\zeta) - 10\mathscr{F}\xi/13, \tag{3.40}$$

where $\mathscr{A}$ and $\mathscr{B}$ are constants and P_{10} and Q_{10} are Legendre function of order 10 of the first and second kind, respectively. The boundary conditions are sufficient to

determine $\mathscr{A}$, $\mathscr{B}$ and $\mathscr{F}$. For $Fr = 1.19$ we have

$$\mathscr{A} = -1.09 \times 10^{-4}, \quad \mathscr{B} = 0 \quad \text{and} \quad \mathscr{F} = 0.214. \tag{3.41}$$

The profiles for $\mathscr{H}(\xi)$ and $\mathscr{U}(\xi)$ are shown in figure 8. The surprising fact is that they are very similar in shape to the functions $H_2(\xi)|_{\sigma=0}$ and $U_2(\xi)|_{\sigma=0}$ but with the opposite sign. At first sight this may appear counterintuitive since the current propagation is more rapid ($\mathscr{F} > 0$) for the polydisperse current than the monodisperse current, and yet the above corrections to the height reduce its value at the nose and reduce the velocity along the length of the current $\mathscr{U} < 0$. To explain the results and unravel this apparent contradiction we observe that the leading-order solutions are the similarity solutions for the intrusion of a gravity current with a constant density and that for these solutions there is an exact balance between the hydrostatic pressure gradient and the inertia of the fluid. Once sedimentation is accounted for this balance is destroyed. Sedimentation occurs most rapidly within the tail of the current where the height is least. Thus the pressure is reduced and the fluid is driven from the tail towards the front of the current. Hence we observe that close to the tail $H_1 < 0$ but close to the nose $H_1 > 0$. The velocity field, U_1 monotonically increases close to the tail, before returning to zero at the front.

The second-order functions for a monodisperse current may be explained as follows. The volume fraction is positive along the entire length of the current, because the first-order correction has over compensated for the effects of sedimentation. Although the first- and second-order functions have a similar profile, they are rather different in magnitude. They have an essentially similar profile because they reflect the pattern of non-uniform sedimentation along the length of the current. (In terms of the variables presented in this study it is the balance between $5s\partial\Omega/\partial s$ and $10\Omega s/HF$.)

For polydisperse currents, we have found that when the flows reach a given length, a smaller proportion of particles will have settled out relative to a monodisperse current with the average settling velocity. This is because the reduced sedimentation velocity of the finest fraction of particles implies that the buoyancy difference between the current and ambient is maintained for longer and hence the currents flows more rapidly. In mathematical terms, we observe that the contribution to Ψ_2 which is proportional to σ^2 is positive. Hence at a given s, the overall volume fraction is higher. We also observe that the speed of the front is greater for a polydisperse current ($\mathscr{F} > 0$). Thus the currents flow faster and further than their monodisperse counterparts. The internal structure of the height and velocity fields associated with a polydisperse current is also somewhat different. Since the sedimentation along the current is reduced, so is the reduction in the hydrostatic pressure gradients. Thus fluid is not accelerated as rapidly from the tail of the current towards the head and fluid does not accumulate at the head to the same extent as the equivalent monodisperse currents. Hence we expect and observe that $\mathscr{U} < 0$ along the entire current and that $\mathscr{H} < 0$ near the front and $\mathscr{H} > 0$ in the tail.

The equation for the propagation of the current correct to $O(s^3)$ can now be written as

$$\dot{s} = s^{2/5}\left[1 - 0.578s + 0.114s^2 + 0.214\sigma^2 s^2 + O(s^3)\right] \quad \text{for} \quad Fr = 1.19. \tag{3.42}$$

This is the shallow-water equivalent of (2.14) and (2.17). As noted above, we conclude that all polydisperse currents travel further than monodisperse currents with the average settling velocity. The effect will be more pronounced in currents driven by suspensions with greater variance in the initial distribution of particle settling velocities, but will be unobserved until $\sigma^2 s^2 \sim 1$. In its present form, the numerical

integration of (3.42) diverges for values of s that exceed one, essentially because the Taylor series is a poor representation of the function $F(s)$ when s becomes of order unity. We could attempt to produce convergent integral approximations, guided by the approximations for the box model (§ 2), but in this section such an approach will not be pursued.

A better approach is provided by rewriting the equation governing the evolution of the volume fraction (3.17) as

$$2(U-\xi)\frac{\partial}{\partial\xi}(\log\Omega)+5s\frac{\partial}{\partial s}(\log\Omega)+\frac{10\,s}{HF}=0. \tag{3.43}$$

We then form a power series for $\log\Omega$ rather than Ω. This is advantageous because the exponential decay of the volume fraction is automatically captured. We find that

$$\log\Omega=\frac{-2}{H_0}s+\frac{5H_1+5F_1H_0-2U_1H_0'}{5H_0^2}s^2+s^3\Omega_3(\xi)+O(s^4). \tag{3.44}$$

The third-order term in this expansion, Ω_3, is determined entirely in terms of the second-order height and velocity fields. Since these are known, it is conceptually simple, though algebraically intensive, to calculate Ω_3. We find that

$$\begin{aligned}\Omega_3=&-\frac{2(-2U_1H_0U_1'H_0'-2H_0U_1^2H_0''+5U_1H_0H_1'-5U_1H_0F_1H_0'+4U_1^2H_0'^2)}{75H_0^3}\\&-\frac{2(-2U_1H_0'H_1+2U_2H_0H_0'-5H_2H_0+5F_1^2H_0^2+5H_1^2-5F_2H_0^2+5F_1H_0H_1)}{15H_0^3}.\end{aligned} \tag{3.45}$$

and henceforth we denote the truncated series for Ω up to and including Ω_3 by $\tilde{\Omega}$.

It is straight-forward to calculate the proportion of particles which have settled out of the flow. Denoting this proportion by p, we find that

$$p=1-\int_0^1 H(\xi,s)\Psi(\xi,s)\,\mathrm{d}\xi. \tag{3.46}$$

To complete our analysis of the shallow-water model of polydisperse gravity currents, we calculate the deposit which arises from their flow. We measure the deposit as the mass per unit area which arises from sedimentation of each class of particles. On the assumption that the density of each class is identical, we non-dimensionalize the deposit with respect to $\rho_p A^{1/2}(\bar{\beta}/5Fr)^{2/5}b^{1/5}\sum_{i=1}^n\phi_i(0)$. (Note that if the particle densities are different then it is still possible to perform this analysis, although the expressions are more complex.) Hence the dimensionless deposit at a downstream location x and a time T is given by

$$\eta(x,T)=\int_{t_*}^{T}2\sum_{i=1}^{n}V_i\varphi_i(x,t)\,\mathrm{d}t\quad\text{for}\quad t_*\geqslant T, \tag{3.47}$$

where $x_N(t_*)=x$. We recast this in terms of the new independent variables, ξ and s, to find

$$\eta=\int_{s_1}^{s_2}\frac{2\sum_{i=1}^{n}V_i\varphi_i(s_1/s,s)}{\dot{s}}\,\mathrm{d}s,\quad s\geqslant s_1, \tag{3.48}$$

where $s_1=[x_N(t_*)]^{5/2}$ and $s_2=s(T)$. The vertical profile of the deposit is also of

interest. We may simply evaluate the proportion of the settling flux associated with each class of particles. Denoting the proportion of the ith class by χ_i, we find,

$$\chi_i(x,T) = \frac{V_i\varphi_i(x,T)}{\sum_{j=1}^{n} V_j\varphi_j(x,T)}. \tag{3.49}$$

Thus both $\chi_i(x,T)$ and $\eta(x,T)$ are known in terms of the expansions developed above and so we may examine the implicit relationship between them to reveal the composition of the deposit at a fixed downstream location x.

3.2. *Comparison with numerical results*

To validate the asymptotic analysis presented above and to determine the regime within which the asymptotic results accurately represent the motion, we numerically integrate the governing equations (3.1)–(3.4), subject to the boundary conditions (3.5)–(3.7). Although our numerical technique could be applied to any number of discrete classes of particles, here we present only the results for bidisperse currents with settling velocities in the ratio 1 : 7. As before we refer to the particulate class with the greater settling velocity as coarse particles and the class with the smaller settling velocity as fine particles. Rather than numerically integrate evolution equations for both classes of particles, it is efficient to note that the volume fraction of the coarse particles, $\phi_1(x,t)$, is known in terms of the volume fraction of the fine particles, $\phi_2(x,t)$, and is given by

$$\phi_1(x,t) = \phi_1(0)\left(\frac{\phi_2(x,t)}{\phi_2(0)}\right)^{\beta_1/\beta_2}. \tag{3.50}$$

The numerical method employed is similar to that developed by Bonnecaze *et al.* (1993) and Hallworth *et al.* (1998). The governing equations were first transformed to employ independent variables (ξ,t). They were then discretized and integrated using a two-step Lax–Wendroff scheme. Some artificial viscosity was added to the momentum equation to preserve the stability of the scheme (see Bonnecaze *et al.* 1993), but this was minimized through extensive testing. The prescribed boundary conditions (3.5)–(3.7) were supplemented by writing the system of equations in characteristic form and determining the characteristics that point out of the computational domain. At each time step the dependent variables were integrated forward in time along the characteristics to provide the additional boundary conditions required for the numerical solution. For the calculations shown here we employed 200 grid points, a timestep 10^{-3} and a dimensionless settling velocity, $\beta_2 = 10^{-3}$. The initial conditions were the similarity solution for the height and velocity fields, given by (3.22) and (3.23) at $t = 0.2$, while the volume fraction was initially set constant throughout the domain. Integration was continued until either $t = 300$ or over 99.9% of the particles had settled out of the suspension.

The scheme was tested in a number of ways. First it was ensured that if both β_1 and β_2 vanished then the numerically calculated solution should reproduce the analytical similarity solution given by (3.22) and (3.23). When $\beta_2 > 0$, the height and velocity fields no longer maintain their similarity form. However for monodisperse flows we have accurate analytical representations of the flow (Harris *et al.* 2001). Thus by setting $\beta_2 = \beta_1$, it was possible to test the accuracy of the numerical scheme. For truly polydisperse flows there are no existing models against which to validate the numerical calculations. However as part of our computations we evaluated the

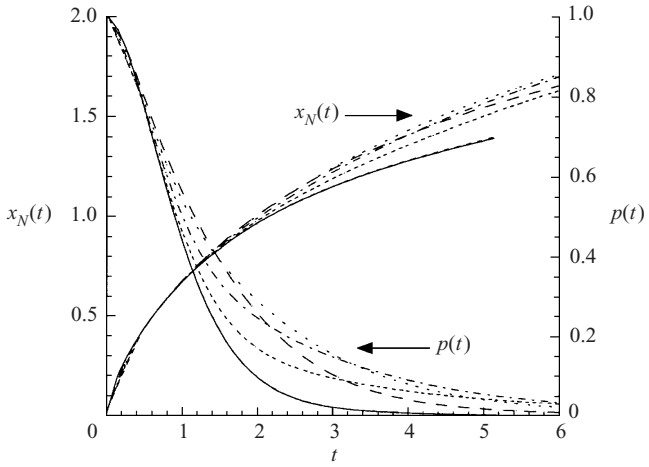

FIGURE 9. The rescaled length (x_N) and proportion of particles in suspension (p) of a particle-driven gravity current containing a bidisperse distribution of particles with a 7 : 1 ratio of settling velocities as a function of time. The different curves correspond to different initial volume fractions of coarse particles: $f = 0$ (———), $f = 0.2$ (– – –), $f = 0.4$ (- - - -), $f = 0.6$ (— · — ·), $f = 0.8$ (· · · · · · ·), $f = 1$ (– – –). (Note that the curves for $f = 0$ and $f = 1$ are indistinguishable.)

volume of fluid moving in the current and found that it was conserved to high accuracy (0.01%). In the results that follow we numerically integrated the governing equations with $\beta_1 = 0.007$ and $\beta_2 = 0.001$ for various initial proportions of coarse and fine particles. As in §2, we denote the proportion of coarse particles by f. We plot the rescaled front position, $x_N(t)$, and the proportion of particles in suspension, $p(t)$, as functions of rescaled time for $f = 0, 0.2, 0.4, 0.6, 0.8$ and 1.0 (figure 9). We note that the curves for $f = 0$ and $f = 1$ are identical as these correspond to monodisperse currents of purely fine and purely coarse particles, respectively. The rescaling (3.8) ensures that these two curves are identical. For $0 \leqslant f \leqslant 1$ we observe that the position of the front, $x_N(t)$ increases faster than for the monodisperse currents and the rate of decrease of the proportion of particle remaining in suspension, $p(t)$ is slower. This indicates that polydisperse currents flow more rapidly than monodisperse currents with the same average settling velocity. This results from the smaller settling velocity of the fine particles in the polydisperse currents which maintain the density difference between the current and the ambient and extend the flow.

We now consider the interior dynamics of the current before returning below to compare our asymptotic formulae with the numerically calculated bulk properties of the flow. We consider the asymptotic form of the velocity and height fields, truncated at $O(s^2)$ and given by

$$\tilde{H} = H_0 + sH_1 + s^2H_2, \tag{3.51}$$

$$\tilde{U} = U_0 + sU_1 + s^2U_2, \tag{3.52}$$

and compare these with the numerically calculated height and velocity fields (figure 10). To illustrate the effects of polydispersion we plot the fields for two flows with initial proportions of coarse particles of 20% and 80%, yielding $\sigma^2 = 1.19$ and 0.17, respectively. The agreement between the asymptotic expressions and the numerical results is reasonable up to $s \approx 1$. It is noteworthy that the polydisperse currents with low and high values of σ^2 adopt rather different profiles as time evolves. For low

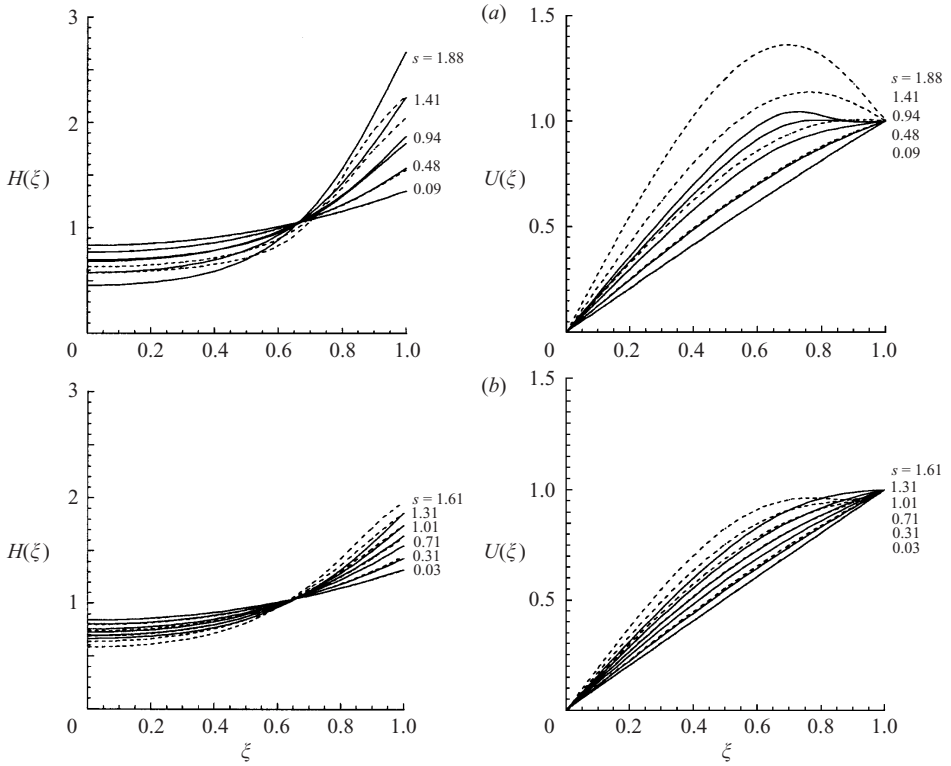

FIGURE 10. The height (H) and velocity (U) fields as functions of ξ within a bidisperse gravity current for different initial proportions of coarse and fine particles: (*a*) $f = 0.8$; (*b*) $f = 0.2$. Results from numerical integration (———) and second-order asymptotic functions (- - - -).

values of σ^2 the current becomes much deeper towards the front than in the rear of flow, as fluid appears to accumulate near the front of the flow. This phenomenon occurs because the settling velocities of the particles have little variation from the mean and so the tail of the current becomes depleted in particles over a short period, thus leading to particle-free fluid accelerating towards the front of the flow. Conversely for flows with a wider range of settling velocities and so a larger σ^2, the particle content in the tail is reduced over an extended period and so the accumulation of particle-depleted fluid at the front is postponed.

Next we consider the volume fraction, using the series expansion for $\log \Omega$, truncated at $O(s^3)$. In figure 11, we plot Ω^{V_2} for two polydisperse flows with $f = 0.2$ and 0.8. We find that the asymptotic theory accurately reproduces the numerical calculations up to times when only relatively small proportions of the initial particles remain in suspension.

In figure 12, we plot the proportion of particles remaining in the current as a function of s. Here the asymptotic expression is calculated from (3.46), using the truncated series representations for H and $\log \Omega$. We plot the curves for a monodisperse current ($\sigma^2 = 0$), a bidisperse current with initially 80% coarse particles ($\sigma^2 = 0.17$) and a bidisperse current with initially 20% coarse particles ($\sigma^2 = 1.19$). We observe that in each case the asymptotic expression yields an accurate estimate of the proportion of particles in suspension up to times when over 95% of them have settled out. This implies that the majority of the motion of the current is accurately modelled by these expansions.

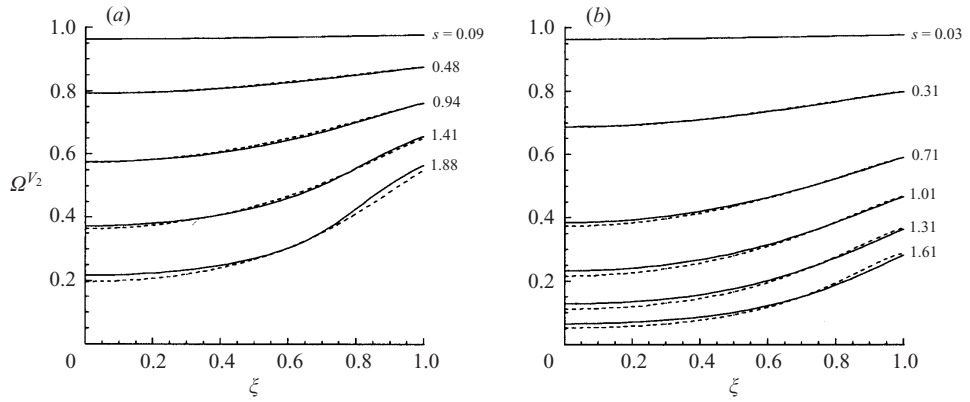

FIGURE 11. The volume fraction (Ω^{V_2}) as a function of ξ within a bidisperse gravity current for different initial proportions of coarse and fine particles: (*a*) $f = 0.8$; (*b*) $f = 0.2$. Results from numerical integration (———) and second-order asymptotic functions (- - - -).

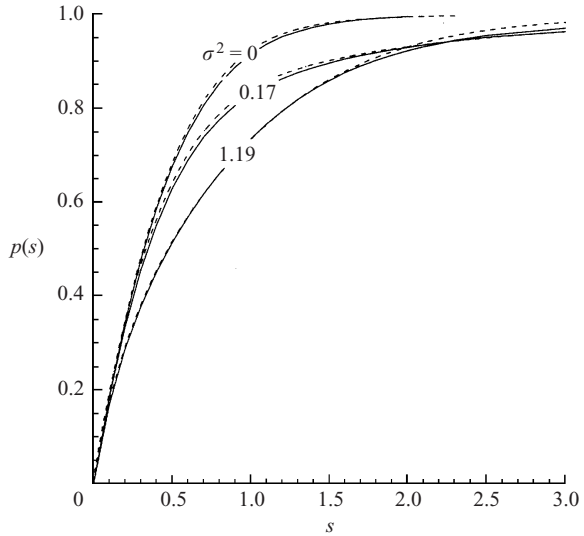

FIGURE 12. The proportion of particles settled from the current (p) as a function of s, for a monodisperse current ($\sigma^2 = 0$), a bidisperse current with $f = 0.8$ ($\sigma^2 = 0.17$) and a bidisperse current with $f = 0.8$ ($\sigma^2 = 1.19$). Results from numerical integration (———) and second-order asymptotic functions (- - - -).

Next we study the length of the current, $x_N(t)$. A stringent test of the accuracy of the asymptotic expressions is to consider $s^{-2/5}\,\mathrm{d}s/\mathrm{d}t \equiv F(s)$ (see (3.11)). We plot in figure 13 the numerically evaluated $s^{-2/5}\,\mathrm{d}s/\mathrm{d}t$ along with the series expansion of $F(s)$ and the improved approximation given by

$$\tilde{F}(s) = \left(b\tilde{H} \sum_{i=1}^{n} \psi_i(0) \tilde{\Omega}^{V_i} \right)^{1/2}. \tag{3.53}$$

We observe that when $s \ll 1$, the power series expansion of $F(s)$ accurately reproduces the numerical calculation, thus validating the series expansion. However the series expansion loses accuracy as s increases. For monodisperse currents the divergence

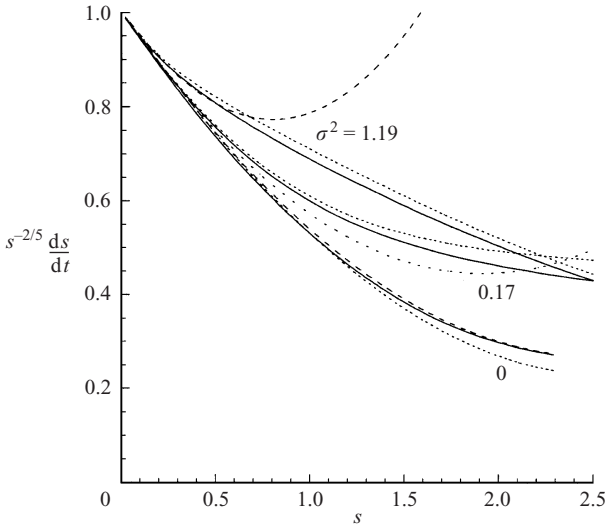

FIGURE 13. Comparison between the numerically evaluated $s^{-2/5}ds/dt$ (———), the truncated power series for $F(s)$ (- - - -) and the approximation $\tilde{F}(s)$ (· · ·) as functions of s for a monodisperse current ($\sigma^2 = 0$), a bidisperse current with $f = 0.8$ ($\sigma^2 = 0.17$) and a bidisperse current with $f = 0.8$ ($\sigma^2 = 1.19$).

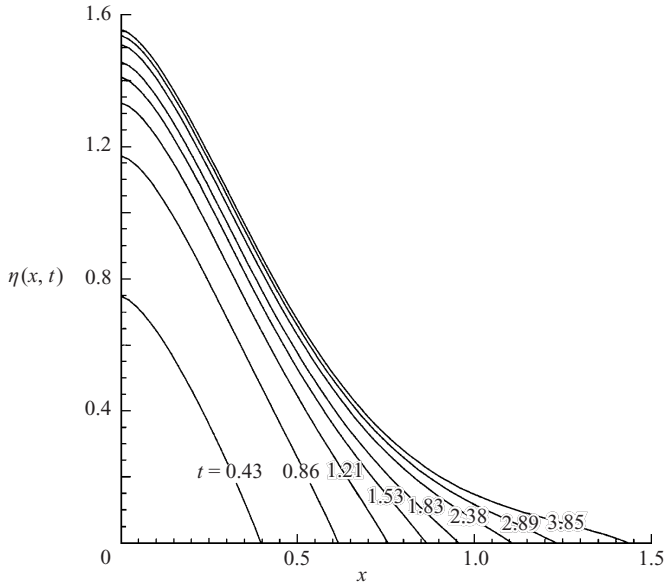

FIGURE 14. The depth of deposit (η) as a function of downstream distance at various times during the evolution of a bidisperse current with $f = 0.5$.

between the two is negligible up to $s \approx 2.5$. However when $\sigma^2 > 0$, the series expansion begins to lose accuracy when $\sigma^2 s^2 \approx 0.5$. This reflects the need to find further terms in the series expansion, which are related to higher-order moments of the initial distribution of particles. However we also note that the approximation $\tilde{F}(s)$ accurately models the evolution of $s^{-2/5}ds/dt$ for s up to 2.5, by which time over 95% of the suspended particles have been deposited from the flow. Consequently the errors in calculating $s(t)$ when $\tilde{F}(s)$ is employed are small (see figure 16).

Initial proportion of coarse particles f	Shallow-water length at 99.5% sedimentation x_r	Box-model length at 99.5% sedimentation L_r	Rescaled box-model length $1.46b^{1/5}L_r$
0	1.35	0.97	1.35
0.2	1.78	1.27	1.77
0.4	2.03	1.43	1.99
0.6	2.21	1.56	2.17
0.8	2.35	1.53	2.12
1	1.35	0.97	1.35

TABLE 1. Comparison between the length of the current when 99.5% of the particles have settled out of the flow using the shallow-water equations and the box model.

We now demonstrate how to use the asymptotic expressions to calculate the deposit which arises from the flow of a polydisperse current. In figure 14 we plot the profiles of the deposit at various times to illustrate how it grows due to progressive sedimentation from the overlying current. However the composition of the current is also evolving in time as the coarse particles settle out first, leaving the fine particles in suspension. Thus deposited particles become progressively finer throughout the current motion. This leads to both vertical and streamwise segregation between the coarse and fine particles within the deposit, even though the flow was generated from an initially well-mixed suspension. In figure 15 we plot the deposit as a function of the rescaled, dimensionless downstream distance from the source, for a bidisperse flow in which there were initially equal proportions of coarse and fine particles ($f = 0.5$). We also plot contours of the proportion of coarse and fine particles within the deposited material, which illustrate how the deposit is segregated both vertically and streamwise.

Finally we compare the numerical calculations for the runout length using the shallow-water equations with the predictions of the box model (§2). To this end we find the distance propagated by the front of the current when, for example, 99.5% of the particles which were initially in suspension have sedimented out of the flow. This length, denoted by x_r, is given as a function of the initial proportion of coarse particles in table 1, where we also present the predictions from the box model, denoted by L_r. Before these values can be compared we must account for two factors. First, the two lengths are non-dimensionalized using different scalings (see (2.13) and (3.8)). Furthermore, studies of the monodisperse flows have found that box models underpredict the lengthscale by a known factor (see Harris *et al.* 2001); using the theoretical framework developed here for a monodisperse flow, we find that, with the same value as used above, 99.5% of the initially suspended particles have settled out of the flow when $s = 2.03$ using the shallow-water equations and $S = 0.93$ using the box model. Together these imply that at this stage of the evolution of the flow, we should multiply the box-model runout length by a factor of $1.46b^{1/5}$. In table 1 we see that although this factor was obtained from calculations for monodisperse flows, it may also be used accurately for the polydisperse flows. Agreement between the two models is worst for flows which have only a relatively small, but non-zero, proportion of fine particles. These flows still have a relatively high average settling velocity and yet the fine particles remain in suspension and accumulate at the front of the current, thus extending the runout length. Box models do not resolve the height profiles of these currents and so cannot reproduce the additional runout due to the accumulation of fine-particle-rich fluid at the front of the flow.

Experiment	Proportion (%) Coarse	Fine	$\bar{\beta}$	Lengthscale (cm)	Timescale (s)
1	0	100	0.0051	502	42.5
2	20	80	0.0120	357	25.5
3	40	60	0.0189	298	19.4
4	50	50	0.0224	279	17.5
5	60	40	0.0258	263	16.1
6	80	20	0.0327	239	14.0
7	100	0	0.0396	221	12.4

TABLE 2. The experimental conditions reported by Gladstone *et al.* (1998). In these experiments, bidisperse mixtures of silicon carbide particles of density $3.22\,\mathrm{g\,cm^{-3}}$ were suspended in water and instantaneously released from behind a lock-gate into a flume of water. The water depth was 40 cm, the lock was of length 20 cm and the flume was of width 20 cm. In each experiment, the initial reduced gravity was $7.58\,\mathrm{cm\,s^{-2}}$. The length- and timescales given in the table are those used to non-dimensionalize the data.

4. Discussion

4.1. *Comparison with experiments*

Gladstone *et al.* (1998) report experiments in which well-mixed bidisperse suspensions of particles were instantaneously released from behind a lock gate into a horizontal flume. They measured the length of the current as a function of time for various initial mixtures of particles (see figure 16 and table 2). The different particles used were of average diameters 25 μm and 69 μm, producing a 1 : 7.7 ratio of settling velocities (calculated using Stokes' settling law). The data have been put in dimensionless terms using the scalings based on an average settling velocity described in § 3. We see that for early times ($t < 2$ and $l < 0.6$) all currents have approximately the same behaviour. This confirms the idea that at early times polydisperse currents behave like monodisperse currents with an average settling velocity. At later times we observe that the curves on this graph of length against time separate out to form a fan (figure 16), which is qualitatively similar to that produced by the models developed in this study (figures 2 and 9). In figure 16 we have also plotted the shallow-water theory for the position of the front as a function of time and the initial fraction of coarse particles. The general agreement between theory and experiment is reasonable although the theory lies ahead of the data for flows with relatively high initial fractions of coarse particles. We investigate this issue below.

The first surprising point is that the curves for the monodisperse currents, driven by either all fine particles or all coarse particles, are rather different, although they should be identical according to the theory (figure 17). There are two possible explanations for this discrepancy (both of which probably play a role). First, the single-layer shallow-water theory does not take into account effects produced by the overlying fluid. Some studies model this effect empirically by including a Froude number condition at the front of the current which is dependent upon the depth of the current relative to the depth of the ambient (see Huppert & Simpson 1980). For the coarse particles, the lengthscale associated with the slumping phase of the current and the lengthscale based on sedimentation, which we have used to scale the data, are rather similar. This means that considerable sedimentation takes place during the slumping phase, during which we need to account for the motion of the overlying ambient fluid. Secondly, at large times the level of turbulence in the flow will have decreased considerably.

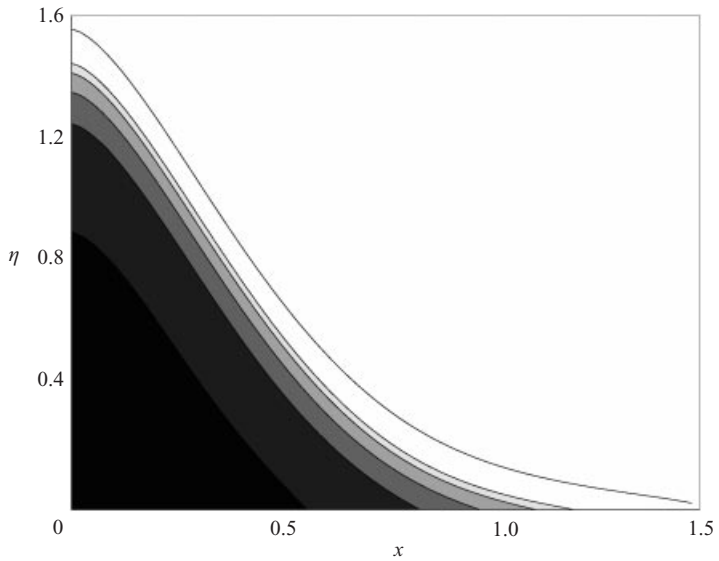

FIGURE 15. The distribution of the deposit and the proportions of coarse and fine particles within it arising from sedimentation from a bidisperse particle-driven gravity current, modelled using the shallow-water equations when the current has reached a length of $s = 3$. In this calculation, the suspension initially contains equal proportions of fine and coarse particles ($f = 0.5$). The contours are shown for 80%, 60%, 40%, 20% and 10% of coarse particles within the deposited material. Also shown is the total depth of the deposit as a function of downstream distance.

The flow may no longer be sufficiently vigorous to maintain the coarse particles in suspension, with the result that the particles are no longer well-mixed throughout the current and so the model of the evolution of the volume fraction should be modified. Thus the current driven by the suspension of coarse particles may propagate less far downstream and may move with a somewhat reduced velocity as seen in figure 17. We find that the results for the current driven by entirely finer particles are well-predicted by the shallow-water model developed in § 3 (see figure 17). We have also integrated the shallow-water equations for lock-release initial conditions, namely $u = 0$ and $h = h_0$ for $0 < x < x_0$, instead of the idealized similarity solution on which the series solutions is based. We find that in terms of the rescaled length and time, there is very little difference between the rates of propagation of these two flows with different initial conditions.

The general collapse of the bidisperse currents is encouraging. The lock-release lengthscale is much less than the sedimentation scale when the initial percentage of fine particles is greater than 20%. For these currents, although the curves of length vs. time lie rather close to each other, the results still confirm the idea that there will be increased propagation in bidisperse currents. In addition, it appears that the runout is greatest for the bidisperse current that contains 60% fine particles, although many of the flows reached the end of the flume before they had fully settled out.

The initial collapse of the currents plays an even more important role in the final pattern of the deposited sediment. Gladstone *et al.* (1998) found that there was a peak in the sedimentation several lock lengths downstream of the release. Pure depositional, shallow-water models seem unable to predict this behaviour correctly. A challenge for the future will be to produce more accurate models of the flow that include sediment erosion as well as deposition. Recent work, using direct numerical simulation, may

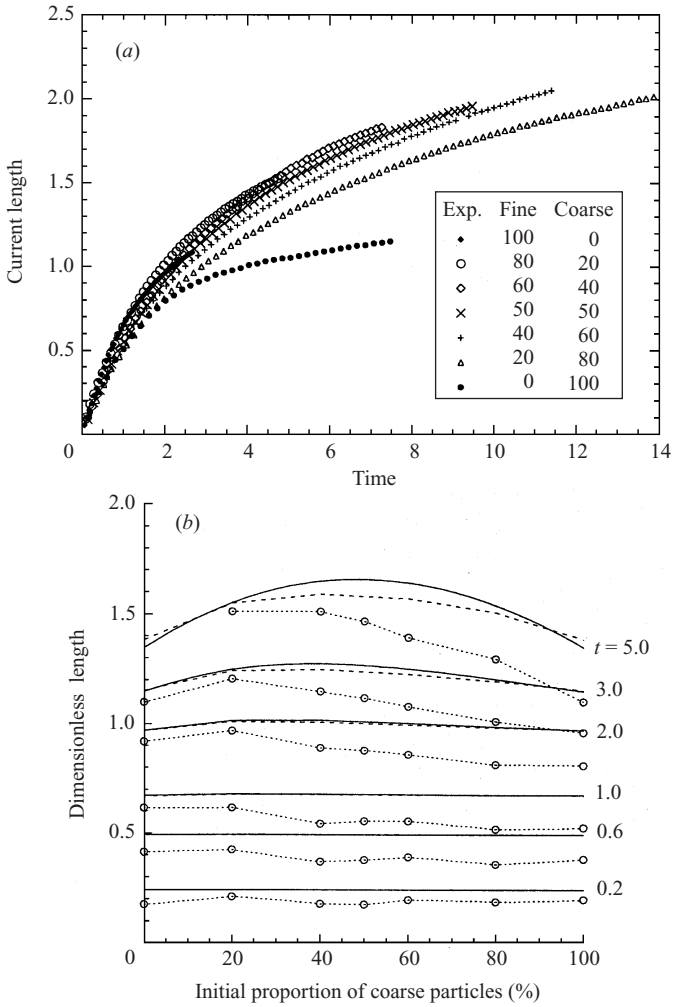

FIGURE 16. Experimental data for the non-dimensional length of bidisperse particle-driven gravity currents released at one end of a channel containing quiescent ambient fluid. The data points (··· ○ ···) are from the experiments of Gladstone *et al.* (1998) and were performed with the same initial aspect ratio and total mass of particles. (*a*) The dimensionless length as a function of the dimensionless time, (*b*) the dimensionless length as a function of the initial volume fraction of coarse particles at $t = 0.2, 0.6, 1.0, 2.0, 3.0, 5.0$. We also plot the results from the numerical integration of the shallow-water equations (———) and asymptotic results (- - - -) at these times.

help to provide a more complete picture. In addition, it would be beneficial to conduct more experiments with differently sized particles, selected to minimize the effect of the lock release process. Effectively this requires that the runout is much greater than the slumping length. So far, we have been constrained by the size of the largest experimental tanks available.

4.2. *Comparison with field observations*

The Northwestern African continental margin has been the focus of considerable study of deep-water sedimentary processes during recent years (Weaver *et al.* 1995; Masson *et al.* 1998; Wynn *et al.* 2002). Within it is located the Moroccan Turbidite System which comprises three interconnected deep-water basins. Large-volume ($>100\,\mathrm{km}^3$)

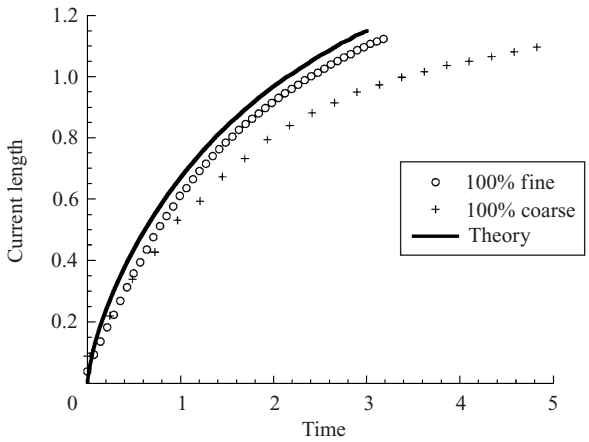

FIGURE 17. Dimensionless length of particle-driven currents composed entirely of coarse particles and entirely of fine particles as a function of time. The experimental data are from Gladstone *et al.* (1998). Also plotted is the theoretical curve (see § 3).

turbidites, sourced from the Moroccan shelf and the volcanic Canary Islands, may travel up to 1500 km before fully depositing their suspended loads. This turbidite system is not only one of the largest in the world but has been extensively cored, permitting the identification of the turbidite along its entire length and yielding significant insight into its depositional structure. In particular, grain size analysis has permitted the calculation of the relative proportions of sand and mud-sized particles within the deposit. Weaver *et al.* (1995) find that the deposit is essentially bidisperse with major fractions of fine sand (100 μm) and mud (2 μm). The proximal deposits exhibit a layer of sand, overlain by mud, whilst the distal deposits are composed entirely of mud. Further analysis of turbidite deposits in this region led Wynn *et al.* (2002) to produce maps of the deposit, indicating the variation of its depth with distance from the source, along with the variation of the composition of the deposited material. We show two schematic pictures of turbidite deposits, as presented by Wynn *et al.* (2002) (figure 18). These lie within the Agadir Basin and arose from a turbidity current emerging from the Agadir Canyon. The basin has regional slopes of up to 0.03°, whilst the canyon is significantly steeper with slopes up to 2° (Wynn *et al.* 2002). The first sketch corresponds to a relatively small turbidite of volume 15 km^3. On entering the deep-water basin it immediately deposits suspended material. The composition of the deposit systematically changes downstream, reducing from a mixture with sand and mud in the ratio 35 : 65 to pure mud in the distal regions. The relatively coarse particles of sand are primarily deposited in a wedge which thins downstream. They are overlain by mud. This pattern is very similar to that predicted by the models of polydisperse flows developed in this study. From an initial mixture of particle sizes, it is possible to form a deposit which is graded in the vertical and in the streamwise direction. The coarse particles settle out first and are then overlain by finer particles (figures 5 and 15).

The larger-volume turbidite (125 km^3) exhibits some similar features, but also some differences. The runout of this flow now exceeds the basin and a significant proportion of the current flows out into the Maderia Abyssal Plain. The deposit thickness does not systematically decrease in the flow direction. Instead the deposit seems to attain a maximum thickness at some distance from the canyon which feeds it. Wynn *et al.*

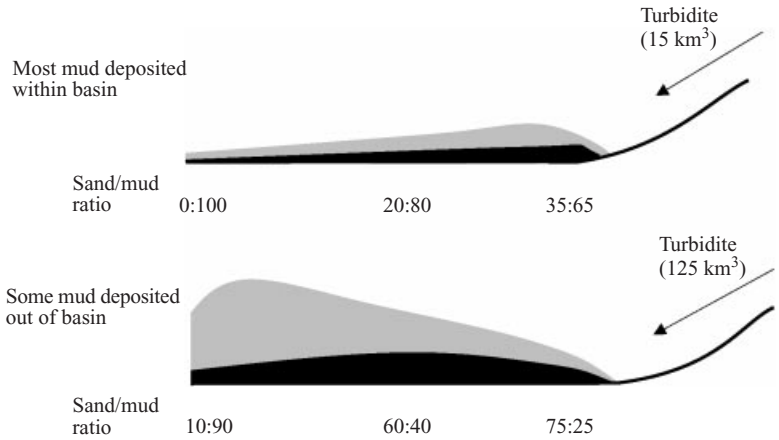

FIGURE 18. Schematic diagram of the depositional architecture of two turbidites in the Agadir basin, after Wynn *et al.* (2002). Diagram not to scale.

(2002) associate this with the large volume of the flow and the high velocity with which it enters the basin. Such high-speed flows may well be erosional and so any deposited material will be re-entrained and advected downstream. However the grain size data suggest that the coarse particles of sand are preferentially deposited, being overlain by a relatively thin layer of mud. As the flow spreads across the relatively flat basin, it slows and becomes depositional.

The models developed here are one-dimensional and although these turbidites are channelized, there is some possibility for lateral spreading. Further the models do not include erosional effects and particles settle out of the flow at a rate which is independent of the bulk velocity. The flows are thus treated as purely depositional and the thickness of the deposit can only decrease in the streamwise direction. However if particle sedimentation is suppressed, or if there is erosion of previously deposited material, then it will be possible to predict distributions of the deposited material which are in accord with these observations. Once the flow speed has dropped so that the flows become purely depositional, the pattern of sedimentation and the composition of the deposit becomes similar to that predicted in this study (figures 5 and 15).

5. Summary and conclusions

In this study we have developed mathematical models of gravity current flows driven by polydisperse suspensions of particles. We have presented two classes of models: 'box' models which are averaged both in the vertical and the streamwise direction and do not resolve the internal structure of the flow, and 'shallow-water' models which elucidate the streamwise variation of vertically averaged properties of the currents. We have demonstrated how flows driven by polydisperse suspensions differ from those driven by an equivalent monodisperse suspension with an average settling velocity. Specifically, if the variance of the initial distribution of settling velocities is much smaller than the square of the mean settling velocity, then it is adequate to assume that the rate of sedimentation of each class of particles to the underlying boundary is independent of each of the other classes. Thus there is no nonlinear interaction between them. This regime leads to the analytical model presented by Bonnecaze *et al.* (1996), which is now fully justified by the analysis developed here.

We have demonstrated theoretically that any degree of polydispersivity adds to the runout length of the currents, relative to that of an equivalent monodisperse currents with an average settling velocity. This occurs because while the coarse particles settle out, the fine particles remain in suspension and thus maintain the density difference between the current and ambient so that the runout length is extended. This is borne out by the experiments of Gladstone *et al.* (1998). By use of the box model we are able to formulate analytical predictions for the runout length of bidisperse suspensions, relative to equivalent monodisperse suspensions with an identical average settling velocity, which is a function of the initial fraction of coarse particles and the ratio of the two settling velocities.

Flows of particle-laden fluid give rise to distributions of deposited particles and we have demonstrated how to calculate the variation of the thickness of the deposit with streamwise distance. The deposit comprises contributions from each class of particles. Not only may we predict the total thickness of each class, but also the variation of the composition of the deposit with depth. Thus we observe how a deposit whose composition varies in both the vertical and streamwise direction may arise from a single, initially well-mixed intrusion of a polydisperse suspension. This prediction is in accord with field observations of turbidite deposits.

Finally we have developed a new analytical scheme for examining the shallow-water model of the flow. This scheme shows how the behaviour of a polydisperse current evolves with time. At early times, it is similar to a compositionally driven current in which the density difference between the current and the ambient fluid remains constant. At later times, particle sedimentation has begun to significantly reduce the overall concentration. At these times, the general characteristics of the current are as if the current were monodisperse, composed of particles with the average settling velocity. The effects of a distribution of settling velocities is only noted at much later times and it is the variance of the initial distribution, relative to the square of the mean settling velocity, which governs its magnitude. The series expansions provide insight into the internal dynamics of the flows and the ways in which the velocity and height adjust to particle sedimentation along the length of the current. We have demonstrated that these series expansions are in good agreement with the results from numerical integration of the shallow-water equations. Finally we have shown how these series expansions may be compared to the box models and hence we may deduce why the seemingly naive box model works well.

This study also suggest future areas of research into the intrusion of particle-laden flows. These include developing a new class of models to resolve the vertical profiles of velocity and particle concentration and the need for further experiments to analyse the effects of a distribution of particle sizes and the composition of the deposit arising from an initially well-mixed flow.

The authors thanks Charlotte Gladstone for making her experimental data available to us and Steve Sparks for useful comments on an earlier draft of this paper. A. J. H. acknowledges the financial support of grants from the Nuffield Foundation (NUFNAL) and the EPSRC.

Appendix. Continuous distribution of particle sizes.

In the main body of this study we pursued 'box' and shallow-water models of the flow of polydisperse gravity currents, driven by a discrete distribution of classes of particles. It is relatively straightforward to generalize this to a continuous distribution

of particle sizes and these are presented in this Appendix. It is possible to derive a shallow-water model for a distribution of particles, but for simplicity we consider only the box model. As in § 2 we denote the length and height of the current by h and l and so conservation of fluid mass gives

$$hl = A, \tag{A1}$$

where A is the volume of fluid per unit width. The volume fraction of particles within the current with sizes between r and $r + \delta r$ is given by $\phi(r,t)\delta r$, where $\phi(r,t)$ specifies the distribution of particle sizes. The settling velocity of the particles in a dilute suspension is a function of their size, shape and excess density relative to the density of the interstitial fluid. For simplicity we assume that the shape and density of the particles are constant so that the settling velocity is only dependent upon the size. (Distributions of density and variations in shape could be incorporated, but the complexity of the analysis would be considerably increased.) Hence we find that the evolution of the volume fraction distribution is given by

$$\frac{\mathrm{d}\phi}{\mathrm{d}t} = -\frac{v_s(r)\phi}{h}. \tag{A2}$$

Finally we have the Froude number condition which expresses the dynamical balance at the front of the current:

$$\frac{\mathrm{d}l}{\mathrm{d}t} = Fr\sqrt{g_p'\Phi h}, \tag{A3}$$

where $\Phi(t) = \int_0^\infty \phi(r,t)\,\mathrm{d}r$. As in §2, the initial conditions are

$$l = 0 \quad \text{and} \quad \Phi = \Phi_0 \equiv \int_0^\infty \phi(r,0)\,\mathrm{d}r \quad \text{at} \quad t = 0. \tag{A4}$$

In terms of the volume fraction distribution function, the average settling velocity is given by

$$\bar{v}_s = \int_0^\infty v_s(r)\phi(r,0)\,\mathrm{d}r. \tag{A5}$$

Henceforth, as in § 2, we non-dimensionalize lengths with respect to $l_\infty = [5FrA(g_p'A)^{1/2}/\bar{v}_s]^{2/5}$, times with respect to $2A/(\bar{v}_s l_\infty)$ and we scale volume fractions by Φ_0. We now denote the dimensionless time by t and the scaled volume fraction distribution by ϕ and introduce $S = [l(t)]^{5/2}$, where $l(t)$ denotes the dimensionless length, to obtain the following equations governing the motion:

$$\frac{\mathrm{d}S}{\mathrm{d}t} = S^{2/5}\gamma(t), \tag{A6}$$

$$\frac{\mathrm{d}\phi}{\mathrm{d}t} = -\frac{2v_s(r)S^{2/5}\phi}{\bar{v}_s}, \tag{A7}$$

where

$$\gamma = \left[\int_0^\infty \phi(r,t)\,\mathrm{d}r\right]^{1/2}. \tag{A8}$$

Finally we write

$$\phi(r,t) = \phi(r,0)a(t)^{v_s(r)/\bar{v}_s}, \tag{A9}$$

and treat a and γ as function of S, rather than t, to find

$$\frac{\mathrm{d}a}{\mathrm{d}S} = -\frac{2a}{\gamma}, \quad \text{with} \quad a(0) = 1. \tag{A10}$$

The formulation of the polydisperse, particle-driven gravity in this way means that it is easy to relate the results to those derived for a monodisperse current and to those for a discrete distribution of particle sizes. We recall from § 2 that for a monodisperse current, $\gamma = 1 - S$, indicating that the current is arrested when $S = 1$. Forming a Taylor series expansion for $\gamma(S)$ in the regime $S \ll 1$, we find that

$$\gamma(S) = 1 - S + \sigma^2 S^2 + \ldots, \tag{A11}$$

where σ^2 is the variance of the distribution of settling velocities, relative to the square of the mean settling velocity, given by

$$\sigma^2 = \int_0^\infty \phi(r,0) \left(\frac{v_s(r)}{\bar{v}_s} - 1 \right)^2 \mathrm{d}r. \tag{A12}$$

The series expansion result (A11), which is identical to (2.17), indicates that the current may be adequately represented by a monodisperse flow with an average settling velocity if $\sigma \ll 1$. Furthermore the early stages of polydisperse flow (when $S \ll 1$) will be similar to an equivalent monodisperse flow with the effects of the distribution being noticeable only at late stages (when $S = O(1)$). However the effect is significant in that any degree of polydispersivity extends the runout of the flow. This is because the particles with lower settling velocities remain in suspension and maintain the flow so that those with larger settling velocities are deposited further from the source.

Finally we note that it is possible to relate the initial distribution of the particle sizes to the runout length of the current. The current attains its maximal runout when $\gamma(S_m) = 0$. Hence

$$S_m = \frac{1}{2} \int_0^1 \frac{1}{a} \left[\int_0^\infty \phi(r,0) a^{v_s(r)/\bar{v}_s} \, \mathrm{d}r \right]^{1/2} \mathrm{d}a. \tag{A13}$$

This integral may be evaluated for any initial distribution of particle sizes, $\phi(r,0)$. It is also possible to expand the integral in terms of moments of the initial distribution of particle settling velocities. We find that

$$S_m = 1 + 2\mathscr{M}_2 - 4\mathscr{M}_3 + 8\mathscr{M}_4 - 12\mathscr{M}_2^2 + \ldots, \tag{A14}$$

where

$$\mathscr{M}_n = \int_0^\infty \phi(r,0) \left(\frac{v_s(r)}{\bar{v}_s} - 1 \right)^n \mathrm{d}r. \tag{A15}$$

We illustrate the use of (A13) by considering an exponential distribution of particle sizes, normalized to have unit mean. Thus the initial distribution is given by

$$\phi(r,0) = \frac{(n+1)^{n+1}}{\Gamma(n+1)} r^n \exp\left(-(n+1)r\right), \tag{A16}$$

where n is a positive constant (see figure 19). This distribution has variance $1/(n+1)$. Thus in the limit $n \to \infty$, the variance vanishes and we recover the result $S_m = 1$. This corresponds to the scaled runout length of a monodisperse gravity current. We integrate (A13) to find the dependence of the runout length on the parameter n which measures the variance of the distribution. By substituting $a = \exp(-v)$ and by assuming that the settling velocity depends quadratically upon the particle radius (Stokes' settling velocity), we find that

$$S_m = \frac{1}{2} \int_0^\infty \left[\int_0^\infty \phi(r,0) \exp(-vr^2) \, \mathrm{d}r \right]^{1/2} \mathrm{d}v. \tag{A17}$$

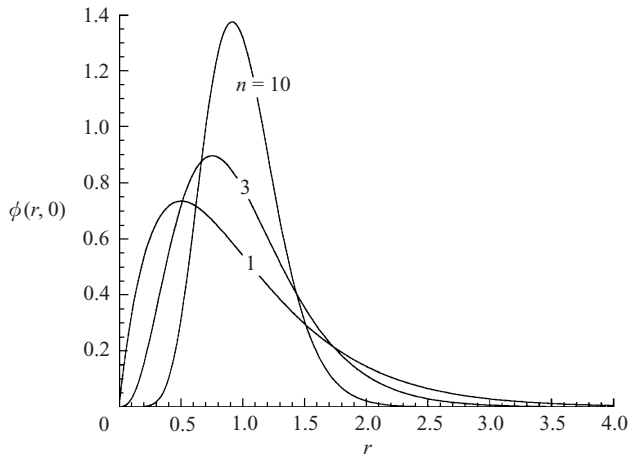

FIGURE 19. Some exponential probability density functions for the initial distribution of particle sizes within a polydisperse current, scaled such that they have unit mean and variance $1/(n+1)$.

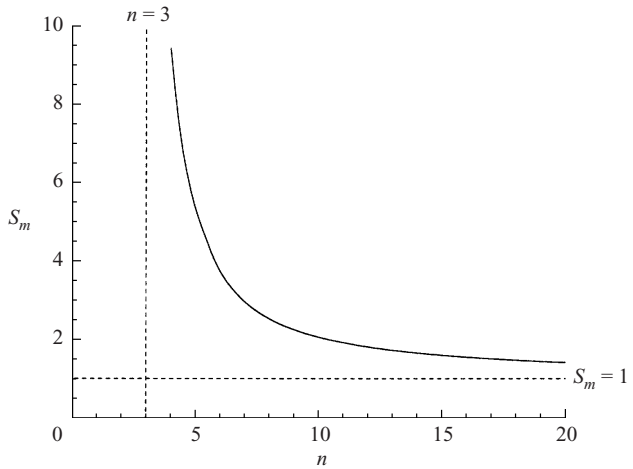

FIGURE 20. The scaled runout distance, S_m, as a function of n, the parameter of the initial exponential distribution of particles sizes.

We note that

$$\int_0^\infty \phi(r,0)\exp(-vr^2)\,\mathrm{d}r \sim \frac{(n+1)^{n+1}\Gamma(\frac{1}{2}(n+1))}{2\Gamma(n+1)v^{(n+1)/2}} \quad \text{as} \quad v \to \infty. \tag{A18}$$

Hence S_m is finite only if $(n+1)/4 > 1$. We have observed before that the presence of fine particles in the flow significantly extends the runout of the current, relative to that expected for a monodisperse current with the average settling velocity. These fine particles sediment more slowly and so remain in suspension longer, thus maintaining the density difference and extending the flow. In the regime $n \leqslant 3$, the variance of the distribution is sufficiently high that there is a significant proportion of very fine particles, with $r \ll 1$, in the initial mixture. Thus the runout is extended to such an extent that it is no longer finite.

We numerically integrate (A13) for $n > 3$ (figure 20). As anticipated we note that as $n \to \infty$, $S_m \to 1$ and that as $n \to 3^+$, $S_m \to \infty$. The key idea these results indicate is

that the runout of a polydisperse gravity current, relative to that of a monodisperse current with the same average settling velocity, is a strong function of the variance of the distribution. Although we have illustrated this only for an exponential distribution of particles, it will also be found for any other initial distribution.

REFERENCES

Abramowitz, M. & Stegun, I. 1964 *A Handbook of Mathematical Functions*. Dover.

Benjamin, T. B. 1968 Gravity currents and related phenomena. *J. Fluid Mech.* **31**, 209–248.

Bonnecaze, R. T., Huppert, H. E. & Lister, J. R. 1993 Particle-driven gravity currents. *J. Fluid Mech.* **250**, 339–369.

Bonnecaze, R. T., Huppert, H. E. & Lister, J. R. 1996 Patterns of sedimentation from polydisperse turbidity currents. *Proc. R. Soc. Lond.* A **452**, 2247–2261.

Dade, W. B. & Huppert, H. E. 1995 A box model for non-entraining suspension-driven gravity surges on horizontal surfaces. *Sedimentology* **42**, 453–471.

Eames, I., Hogg, A. J., Dalziel, S. B. & Gething, S. J. 2001 Erosion by gravity currents. *J. Geophys. Res.* **106**, 14095–14111.

Fredsoe, J. & Deigaard, R. 1992 *Mechanics of Coastal Sediment Transport*. World Scientific.

Gladstone, C., Philips, J. C. & Sparks, R. S. J. 1998 Experiments on bidisperse, constant-volume gravity currents: propagation and sediment deposition. *Sedimentology* **45**, 833–843.

Gladstone, C. & Woods, A. W. 2000 On the application of box-models to particle-driven gravity currents. *J. Fluid Mech.* **416**, 187–195

Hallworth, M. A., Hogg, A. J. & Huppert, H. E. 1998 Effects of external flow on compositional and particle gravity currents. *J. Fluid Mech.* **359**, 109–142.

Hallworth, M. A. & Huppert, H. E. 1998 Abrupt transitions in high-concentration, particle-driven gravity currents. *Phys. Fluids* **10**, 1083–1087.

Harris, T. C., Hogg, A. J. & Huppert, H. E. 2001 A mathematical framework for the analysis of particle-driven gravity currents. *Proc. R. Soc. Lond.* A **457**, 1241–1272.

Hogg, A. J., Ungarish, M. & Huppert, H. E. 2000 Particle-driven gravity currents: asymptotic and box-model solutions. *Eur. J. Mech.* B **338**, 139–165.

Hoult, D. P. 1972 Oil spreading on the sea. *Annu. Rev. Fluid Mech.* **4**, 341–368.

Huppert, H. E. 1998 Quantative modelling of granular suspension flows. *Phil. Trans. R. Soc. Lond.* A **356**, 2471–2496.

Huppert, H. E. & Simpson, J. E. 1980 The slumping of gravity currents. *J. Fluid Mech.* **99**, 785–799.

Martin, D. & Nokes, R. 1988 Crystal settling in a vigorously convecting magma chamber. *Nature* **332**, 534–536.

Masson, D. G., Canals, M., Alonso, B., Urgeles, R. & Huhnerbach, V. 1998 The canary debris flows: source area morphology and failure mechanisms. *Sedimentology* **45**, 411–432.

Simpson, J. E. 1997 *Gravity Currents in the Environment and the Laboratory*, 2nd Edn. Cambridge University Press.

Sparks, R. S. J., Bursik, M. I., Carey, S. N., Gilbert, J. S., Glaze, L. S., Sigurdsson, H. & Woods, A. W. 1997 *Volcanic Plumes*. Wiley.

Weaver, P. P. E., Masson, D. G., Gunn, D. E., Kidd, R. B., Rothwell, R. G. & Maddison, D. A. 1995 Sediment mass wasting in the canary basin. In *Atlas of Deep Water Environments: Architectural Style in Turbidite Systems* (ed. K. T. Pickering, R. N. Hiscott, N. H. Kenyon, F. Ricci Lucchi & R. D. A. Smith), pp. 287–297. Chapman and Hall.

Wynn, R. B., Weaver, P. P. E., Masson, D. G. & Stow, D. A. V. 2002 Turbidite depositional architecture across three interconnected deep-water basins on Northwest African margin. *Sedimentology*. **49**, 661–695.